



Supplement of

Indicators of Global Climate Change 2023: annual update of key indicators of the state of the climate system and human influence

Piers M. Forster et al.

Correspondence to: Piers M. Forster (p.m.forster@leeds.ac.uk)

The copyright of individual parts of the supplement might differ from the article licence.

S1. Context

The IPCC Special Report on Global Warming of 1.5°C (SR1.5), published in 2018, provided an assessment of the level of human-induced warming and cumulative emissions to date (Allen et al., 2018) and the remaining carbon budget (Rogelj et al., 2018) to support the evidence base on how the world is progressing in terms of meeting aspects of the Paris Agreement. The AR6 WGI Report, published in 2021, assessed past, current and future changes of these and other key global climate indicators, as well as undertaking an assessment of the Earth’s energy budget. It also updated its approach for estimating human-induced warming and global warming level. In AR6 WGI and here, reaching a level of global warming is defined as the global surface temperature change, averaged over a 20-year period, exceeding a particular level of global warming, e.g. 1.5°C global warming. Given the current rates of change and the likelihood of reaching 1.5°C of global warming in the first half of the 2030s (Lee et al., 2021; Lee et al., 2023; Riahi et al., 2022), it is important to have robust, trusted, and also timely climate indicators in the public domain to form an evidence base for effective science-based decision making.

S2. Emissions

Table S1 Coverage of UNFCCC F-gases across datasets shown in Figure 2 of the main manuscript

Species	PRIMAP CR v2.5.1	PRIMAP TP v2.5.1	EDGAR v8.0	CIP 2024.04	Annex I Inventories
NF3	x	x	x	x	x
SF6	x	x	x	x	x
Perfluorocarbons (PFCs)					
CF4			x	x	x
C2F6			x	x	x
C3F8			x	x	x
C4F10			x	x	x
c-C4F8			x	x	x
C5F12			x	x	x

C6F14			X		X		X
C7F16					X		
C8F18					X		
C10F18							X
c-C3F6							X
PFC Basket	X			X			X
Hydrofluorocarbons (HFCs)							
HFC-23			X		X		X
HFC-32			X		X		X
HFC-41			X				X
HFC-43-10mee			X		X		X
HFC-125			X		X		X
HFC-134			X				X
HFC-134a			X		X		X
HFC-143			X				X
HFC-143a			X		X		X
HFC-152							X
HFC-152a			X		X		X
HFC-161							X
HFC-227ea			X		X		X
HFC-236cb							X
HFC-236ea					X		X
HFC-236fa			X				X
HFC-245ca							X
HFC-245fa			X		X		X

HFC-365mfc

X

X

X

HFC Basket

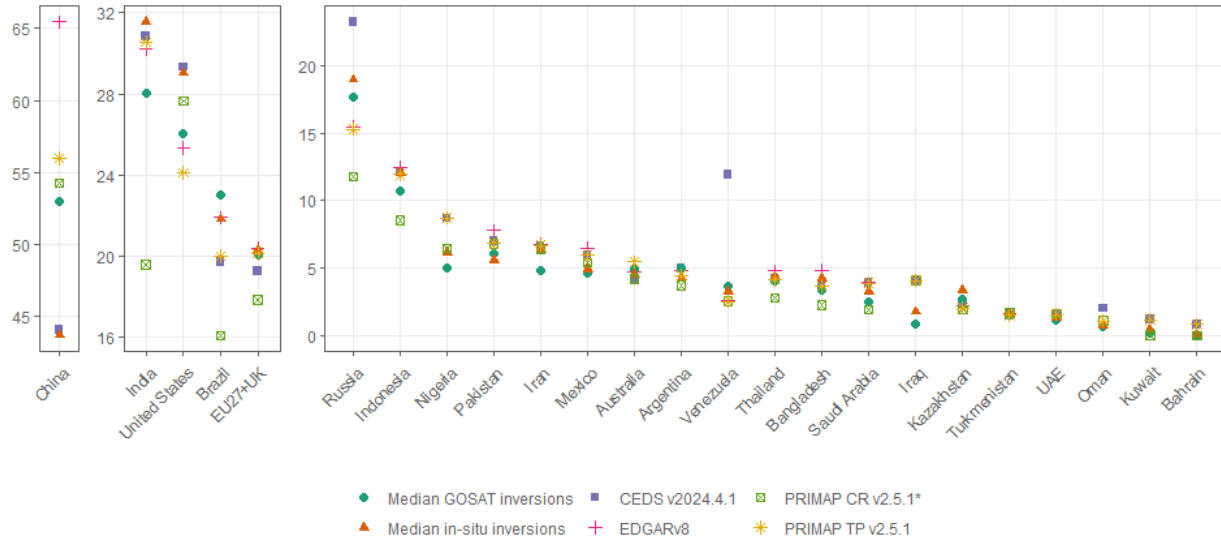
X

X

X

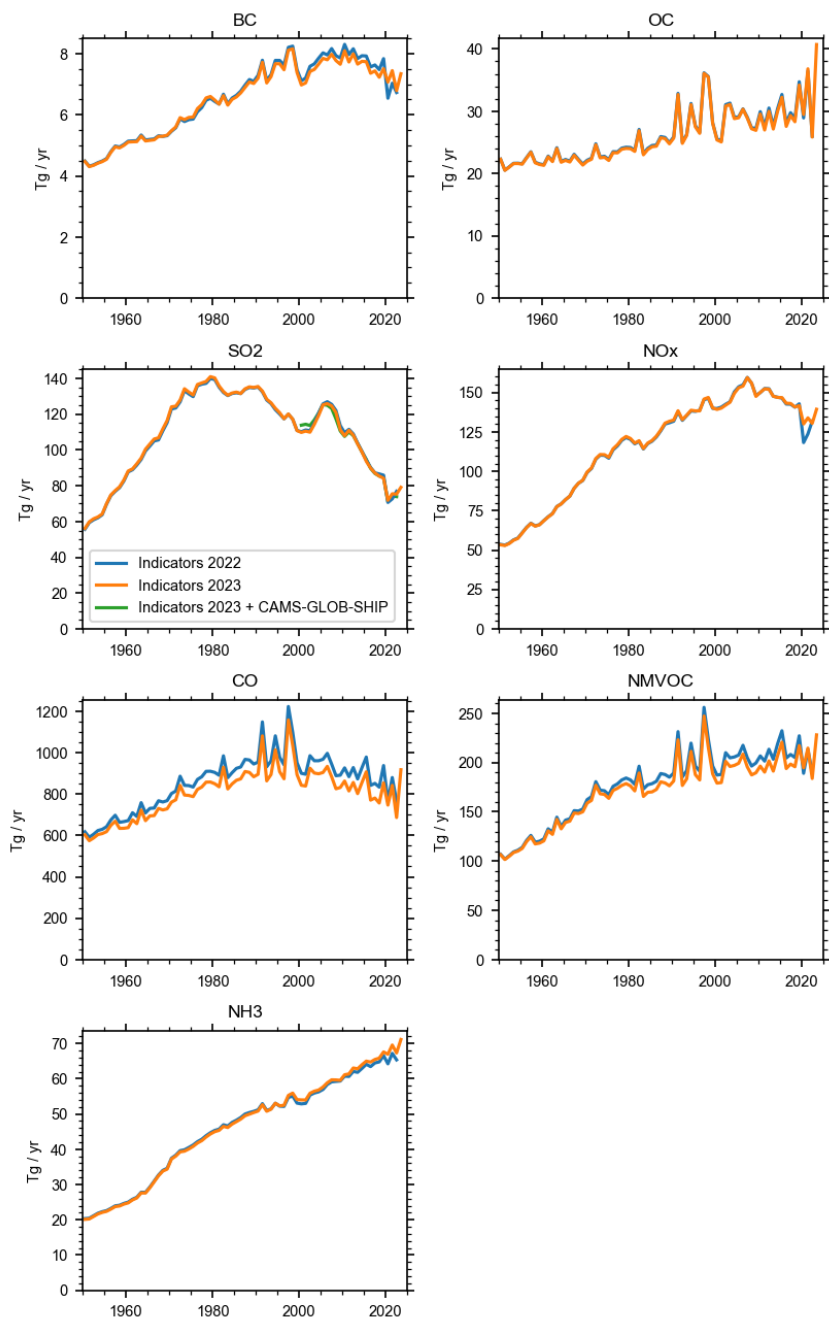
Total anthropogenic CH₄ emissions by country and dataset

Mt CH₄/year (2010-2017 average)



15

Figure S1 Total anthropogenic CH₄ emissions by country and dataset. Median GOSAT and in-situ inversions are sourced from Deng et al. 2022, using the “Method 1” approach of partitioning natural and anthropogenic CH₄ fluxes (excluding biomass fires). See Sect. 2.1 for a list of other datasets.



20

Figure S2 Comparison of short-lived climate forcer emissions from Forster et al. (2023) (blue) using a COVID-derived extension for 2020-22 for fossil, industrial & agricultural sectors, this years' estimates (orange) from an update to CEDS through 2022, and this

years' estimate for shipping SO₂ emissions replaced with those from CAMS-GLOB-SHIP (green). (Granier et al. 2019; Jalkanen et al. 2012, 2016; Johansson et al., 2017).

25 S3. Greenhouse gas concentrations

Naming conventions and details for Sect. 3 of the main paper and herein follow AR6 WGI Chapter 2 (Gulev et al., 2021).

Table S2 Annual mean concentrations of well-mixed greenhouse gases in 2023, 2022, 2019, 1850 and 1750. Except for CO₂, CH₄ and N₂O, concentrations all are in parts per trillion by volume [ppt]. For halogenated gases, concentrations are stated for each gas, with equivalents for HFCs, PFCs and Montreal gases given as the radiative equivalent of the most abundant gas in each category.

Greenhouse gas	1750	1850	2019	2022	2023
CO ₂ [ppm]	278.3	285.5	410.1	417.1	419.3
CH ₄ [ppb]	729.2	807.6	1866.3	1911.8	1922.5
N ₂ O [ppb]	270.1	272.1	332.1	335.9	336.9
NF ₃	0	0	2.1	2.7	2.9
SF ₆	0	0	10.0	11.0	11.4
SO ₂ F ₂	0	0	2.5	2.8	2.9
HFCs as HFC-134a-eq	0	0	237.1	2855	301.4
HFC-23	0	0	32.4	35.9	36.9
HFC-32	0	0	20.0	27.7	30.5
HFC-125	0	0	29.4	40.1	43.5
HFC-134a	0	0	107.6	124.4	129.5
HFC-143a	0	0	24.0	29.2	31.2
HFC-152a	0	0	7.1	7.4	7.6
HFC-227ea	0	0	1.6	2.1	2.3
HFC-236fa	0	0	0.2	0.2	0.2
HFC-245fa	0	0	3.1	3.9	4.2
HFC-365mfc	0	0	1.1	1.1	1.1
HFC-43-10mee	0	0	0.3	0.3	0.3
PFCs as CF ₄ -eq	34	34	109.7	114.4	115.3
CF ₄	34	34	85.6	88.5	89.5
C ₂ F ₆	0	0	4.8	5.2	5.2
C ₃ F ₈	0	0	0.7	0.7	0.8
c-C ₄ F ₈	0	0	1.8	1.9	2.0
n-C ₄ F ₁₀	0	0	0.2	0.2	0.2
n-C ₅ F ₁₂	0	0	0.1	0.2	0.2

n-C ₆ F ₁₄	0	0	0.2	0.2	0.2
i-C ₆ F ₁₄	0	0	0.1	0.1	0.1
C ₇ F ₁₆	0	0	0.1	0.1	0.1
C ₈ F ₁₈	0	0	0.1	0.1	0.1
Montreal gases as CFC-12-eq	8.5	8.5	1032.0	1012.6	1004.3
CFC-11	0	0	226.2	219.3	217.0
CFC-12	0	0	503.1	491.4	487.2
CFC-112	0	0	0.4	0.4	0.4
CFC-112a	0	0	0.1	0.1	0.1
CFC-13	0	0	3.3	3.4	3.4
CFC-113	0	0	69.8	68.1	67.6
CFC-113a	0	0	0.9	1.2	1.3
CFC-114	0	0	16.0	16.0	16.0
CFC-114a	0	0	1.0	1.0	1.0
CFC-115	0	0	8.7	8.8	8.8
HCFC-22	0	0	246.8	248.7	247.3
HCFC-31	0	0	0.1	0.1	0.1
HCFC-124	0	0	1	0.9	0.9
HCFC-133a	0	0	0.4	0.4	0.4
HCFC-141b	0	0	24.4	24.6	24.5
HCFC-142b	0	0	22.2	21.4	21.2
CH ₃ CCl ₃	0	0	1.6	1.1	1.0
CCl ₄	0	0	77.9	75.0	73.8
CH ₃ Cl	457	457	544.2	545.6	548.0
CH ₃ Br	5.3	5.3	6.5	6.6	6.5
CH ₂ Cl ₂	6.9	6.9	40.6	41.0	41.0
CHCl ₃	4.8	4.8	8.8	9.0	9.0
Halon-1211	0	0	3.3	3.0	2.9
Halon-1301	0	0	3.3	3.3	3.3
Halon-2402	0	0	0.4	0.4	0.4

S4. Effective radiative forcing (ERF)

S4.1 Well-mixed greenhouse gas ERF methods

Radiative forcing (RF) from CO₂, CH₄ and N₂O use the simplified formulas from concentrations in Meinshausen et al. (2020), derived from an updated functional fit to Etminan et al. (2016) line-by-line radiative transfer results. These formulas are, to first order, logarithmic with CO₂ concentrations and a square-root dependence for CH₄ and N₂O, with additional corrections and radiative band overlaps between gases. RF is converted to ERF using scaling factors (1.05, 0.86 and 1.07 for CO₂, CH₄, N₂O respectively) that account for tropospheric and land-surface rapid adjustments (Smith et al., 2018a; Hodnebrog et al., 2020a). ERF from other GHGs is assumed to scale linearly with their concentration based on their radiative efficiencies expressed in W m⁻² ppb⁻¹ (Hodnebrog et al., 2020b, Smith et al., 2021b). A scaling factor translating RF to ERF is implemented for CFC-11 (1.13) and CFC-12 (1.12) (Hodnebrog et al., 2020a), whereas no model evidence exists to treat ERF differently to RF for other halogenated gases.

Relative uncertainties in the ERF for CO₂ ($\pm 12\%$), CH₄ ($\pm 20\%$) and N₂O ($\pm 14\%$) are unchanged from AR6. These stem from a combination of spectroscopic uncertainties and uncertainties in the adjustment terms converting RF to ERF; uncertainties in the volume mixing concentrations themselves are assessed to be small (Sect. 2.2). Uncertainties in the ERF from halogenated gases are treated individually and are assessed as $\pm 19\%$ for gases with a lifetime of 5 or more years and $\pm 26\%$ for shorter lifetime gases. In AR6, a $\pm 19\%$ uncertainty was applied to the sum of the ERF from all halogenated gases. To maintain a consistent uncertainty range across the sum of ERF from halogenated gases with AR6, we inflate the uncertainty in each individual gas by a factor of 2.05. Uncertainties are applied by scaling the full ERF time series for each gas.

S4.2 Aerosol ERF methods

Aerosol ERF is a combination of contributions from aerosol-radiation interactions (ERFari) and aerosol-cloud interactions (ERFaci).

S4.2.1 Aerosol-radiation interactions

Contributions to ERFari are assumed to scale linearly with certain SLCF emissions in Sect. 2.3 (SO₂, BC, OC, NH₃, NO_x and VOC) or concentrations (CH₄, N₂O and ozone-depleting halocarbons) of primary aerosols and chemically active precursor species. The coefficients converting emissions or concentrations of each SLCF into ERF and its uncertainty come from Chapter 6 of AR6 WGI (Szopa et al., 2021), originally from CMIP6 AerChemMIP models (Thornhill et al., 2021a). We scale these

coefficients to reproduce the headline AR6 WGI ERFari assessment of -0.3 W m^{-2} from 1750 to 2005-2014. Uncertainties are applied as a scale factor for each species and applied to the whole time series.

60

The inclusion of more species that affect ERFari differs from the AR6 WGI calculation of ERFari in Chapter 7, which only used SO_2 , BC, OC and NH_3 (Smith et al., 2021b). In the update, these four species remain the dominant aerosol and aerosol precursors. Additionally, these coefficients have changed slightly due to switching to CMIP6 era data. In AR6, the coefficients scaling emissions to ERF for SO_2 , BC, OC and NH_3 were provided by CMIP5-era models (Myhre et al., 2013a). The additional
65 coefficients and slight changes to their magnitude had an imperceptible effect on the results but have been included to align with current best practice. This might be important in future years as NO_x and VOC precursors might make up a larger fraction of ERFari.

S4.2.2 Aerosol-cloud interactions

ERFaci is estimated by assuming a logarithmic relationship with the change in cloud droplet number concentration (CDNC)

70

$$\text{ERFaci} = \beta \log(1 + \Delta\text{CDNC}) \quad (\text{S1})$$

$$\Delta\text{CDNC} = s_{\text{SO}_2}\Delta E_{\text{SO}_2} + s_{\text{BC}}\Delta E_{\text{BC}} + s_{\text{OC}}\Delta E_{\text{OC}} \quad (\text{S2})$$

75 where s_{SO_2} , s_{BC} and s_{OC} are sensitivities of the change in CDNC with the change in emissions of SO_2 , BC and OC respectively (ΔE). This relationship is fit to estimates of ERFaci in 13 CMIP6 models contributing results to the piClim-histaer and histSST-piAer experiments of RFMIP and AerChemMIP, respectively, to CMIP6. The ERFaci in these 13 models is estimated using the Approximate Partial Radiative Perturbation (APRP) method (Taylor et al., 2007; Zelinka et al., 2014).

80 The s_{SO_2} , s_{BC} and s_{OC} values from each model are combined into a kernel density estimate and sampled 100,000 times to provide a CMIP6-informed distribution of these parameters. To obtain β for each sample given $(s_{\text{SO}_2}, s_{\text{BC}}, s_{\text{OC}})$ a target ERFaci value for 1750 to 2005-2014 is drawn from the headline AR6 distribution of -1.0 [-1.7 to -0.3] W m^{-2} and eq. (S1) rearranged. This follows a very similar procedure to AR6 and is based on Smith et al. (2021a) with three updates. Firstly, the relationships in eqs. (S1) and (S2) are slightly updated and simplified. Secondly, an additional two CMIP6 models have become available
85 since the AR6 WGI assessment which expands the sampling pool for coefficients from 11 to 13. Thirdly, a slight error in computing ERFaci from APRP from the CMIP6 models in Smith et al. (2021a) has been corrected (Zelinka et al., 2023).

Unlike in the 2022 Indicators (Forster et al. 2023), the update to CEDS means that we do explicitly include the reduction in SO₂ shipping emissions from the introduction of the International Maritime Organization (IMO) convention on sulphur content in fuel in this year's dataset. As we show in Fig. S2, the proxy estimate from Forster et al. (2023), based on activity data during COVID-19 (Forster et al. 2020; Lamboll et al. 2021) was a very good approximation of the latest best estimate from CEDS, and thus the global emissions sum has not changed substantially for 2019-2022 between dataset versions. As a sensitivity case we include an alternative estimate of shipping SO₂ emissions from CAMS-GLOB-SHIP (Jalkanen et al. 2012, 2016; Johansson et al., 2017) for the 2000-2022 period (green line in Fig. S2). The shipping SO₂ reduction in CAMS-GLOB-SHIP dataset from 2019 to 2020 is 8.3 TgSO₂, compared to 7.4 TgSO₂ in CEDS. At the global level, the difference is small in terms of total SO₂ emissions. Unlike the majority of anthropogenic emissions which are land-based, shipping emits primarily in oceanic regions. Ship tracks very readily form in oceanic shallow stratocumulus regions (Watson-Parris et al., 2022) and the reduction of sulphate aerosol (an efficient cloud condensation nuclei) may reduce the magnitude (increase the positivity) of ERF_{aci} more so than an equivalent reduction in emissions from another sector. One estimate of the role of the ship emission change over 2020 to 2023 from the change in sulphur regulation puts the ERF increase at $+0.12 \pm 0.03 \text{ W m}^{-2}$ (Gettelman et al., 2024; see also Yuan et al. 2022). This is similar to the ERF change resulting from the 7.4 TgSO₂ change applied in this study which gives roughly $+0.09 \text{ W m}^{-2}$, computed by linearly scaling the ERF_{aci}. The evidence for a different efficacy of ship-track SO₂ emissions compared to land-based SO₂ emissions should be considered and this will be reviewed in future should further research emerge.

105 **S4.3 Ozone ERF methods**

Ozone ERF is derived from CMIP6 model-based estimates. As in AR6 WGI Chapter 7, we use results from ESMs and chemical transport models that produced historical ozone RF estimates in Skeie et al. (2020). We use only the six ESMs in Skeie et al. (2020) that are independent, include stratospheric and tropospheric ozone chemistry, and produce observationally plausible distributions of present-day ozone (Smith et al., 2021b). From these model time series of ozone RF from 1850 to 2014, we infer the sensitivity of ozone RF to emissions of NO_x, VOC and CO, concentrations of CH₄, N₂O and ozone-depleting halogens, and global mean surface temperature (GMST) anomaly. The fit of the precursor sensitivities and GMST is performed using a least-squares curve fit, with the search bounds of each coefficient set to the 90% range (1.645 times standard deviation) of each species' contribution to ozone forcing determined using single-forcing experiments in Thornhill et al. (2021a) from a number of CMIP6 models contributing to AerChemMIP. UKESM1-0-LL has an anomalously large stratospheric ozone depletion response to halocarbons (Keeble et al., 2021), so this model was excluded when constructing these ranges. In CMIP6, experimental results that vary CO and VOC emissions separately are not available, so individual contributions from CO and VOC to the CO+VOC total are based on their fractional contributions from ACCMIP (CMIP5-era) models in Stevenson et al. (2013). For the global mean temperature contribution, we use the model responses to ozone forcing per degree warming in

chemistry-enabled models in abrupt-4xCO₂ experiments (Thornhill et al., 2021b). Following AR6, we do not differentiate
120 between stratospheric and tropospheric ozone, and we also assume that ERF is the same as RF as there is limited model
evidence to suggest otherwise.

S4.4 ERF from other anthropogenic forcings

Minor categories of anthropogenic forcings include contributions from land use and land use change other than via GHG
emissions, aviation contrails and contrail-induced cirrus, stratospheric water vapour from methane oxidation, and light
125 absorbing particles on snow and ice.

The methodology to estimate ERF from land use and land-use change has been updated to use a scale factor with cumulative
CO₂-LUC emissions since 1750. This provides a similar time history to the land use ERF in AR6 and links this directly to land
use ERF in future scenarios (Smith et al., 2021b). We anchor the 1750-2019 assessment to be the same as AR6 at -0.20 [-0.30
130 to -0.10] W m⁻² under this updated methodology. With this, albedo changes and effects of irrigation (mainly via low-cloud
amount) are accounted for, while other biogeophysical effects of land use and land-use change are deemed to be of second-
order importance (Smith et al., 2021b).

Stratospheric water vapour from methane oxidation was assessed to be 0.05 [0.00 to 0.10] W m⁻² in AR6 for 1750-2019. We
135 use the same scale factor applied to methane ERF used in AR6.

The ERF from light absorbing particles on snow and ice (LAPSI) is assumed to scale with emissions of black carbon. As in
AR6, the contribution from brown carbon is assumed to be negligible. We align the coefficient that converts BC emissions to
ERF from LAPSI to be 0.08 [0.00 to 0.18] W m⁻² for 1750-2019.

140

To estimate ERF from aviation contrails and contrail-induced cirrus in AR6, emissions of NO_x from the aviation sector in
CEDS were scaled to reproduce an ERF of 0.0574 [0.019 to 0.098] W m⁻² for 1750-2018 as assessed in Lee et al. (2021). We
more closely follow the original methods of Lee et al. (2021) in this update to base our ERF estimates as closely as possible
on aviation activity data. The Lee et al. (2021) ERF time series is extended to 2019 based on aviation fuel consumption from
145 the International Energy Agency's (IEA) World Oil Statistics (2022). For 2020, 2021 and 2022, we use fuel consumption data
from the International Air Transport Association (IATA, 2022).

S4.5 Methods for estimating natural forcing

Natural forcing is composed of solar irradiance and volcanic eruptions.

S4.5.1 Solar irradiance

150 The method to compute solar forcing is unchanged from AR6, using a composite time series prepared for PMIP4 (Junglaus et al., 2017) and CMIP6 (Matthes et al., 2017). The headline assessment of solar ERF is based on the most recent solar cycle (2009-2019), which is unchanged from AR6. Solar ERF estimates are computed relative to complete solar cycles encompassing the full “pre-industrial” period where proxy data exists (6754 BCE to 1745 CE).

S4.5.2 Volcanic

155 Volcanic ERF consists of contributions from stratospheric sulphate aerosol optical depth (sAOD; a negative forcing) and stratospheric water vapour (sWV, a positive forcing). The sAOD time series (at a nominal wavelength of 550 nm) is constructed from a combination of four datasets which have temporal overlap. We use ice-core deposition data from HolVol v1.0 (Sigl et al., 2022) for 9500 BCE to 1900 CE. This has been extended backwards in time from the equivalent dataset used in AR6 (eVolv2k; Toohey and Sigl, 2017) which had temporal coverage of 500 BCE to 1900 CE. For 1850 to 2014 we use the CMIP6
160 volcanic sAOD dataset (Dhomse et al., 2020). Since 1979, the CMIP6 dataset was constructed using the Global Space-based Stratospheric Aerosol Climatology (GloSSAC) v1.0 (Thomason et al., 2018). We use an updated, extended version of GloSSAC (v2.2) providing sAOD up to 2021, which is itself an extension of the version used in AR6 (v2.0) ending in 2018 (Kovilakam et al., 2020). The 525 nm extinction from GloSSAC is used and converted to 550 nm using an Ångstrom exponent of -2.33. For 2013 to 2022, we use the Ozone Mapping and Profiling Limb Profiler (OMPS LP) Level 3 aerosol optical depth
165 at 745 nm, which is scaled to achieve the same time mean sAOD as GloSSAC in the overlapping 2013-2021 period as a single Ångstrom exponent is not suggested for this conversion. The 745 nm band is used as this is reported to be more stable than the bands closer to 550 nm from OMPS LP (Taha et al., 2021). Other than for the 2013-2021 overlap between GloSSAC v2.2 and OMPS LP in which only GloSSAC is used, we use a cross-fading approach to blend datasets in overlapping periods. Differences between datasets are minimal. sAOD is converted to a radiative effect using a scaling factor of -20 ± 5 as in AR6
170 (Smith et al., 2021b) that is representative of CMIP5 and CMIP6 models. Effective radiative forcing is calculated with reference to the change in this radiative effect since “pre-industrial”, defined as the mean of all available years before 1750 CE. In other words, the mean of the pre-1750 period is defined as zero forcing.

The January 2022 eruption of Hunga Tonga-Hunga Ha’apai (HTHH) was an exceptional episode in that it emitted large
175 amounts of water vapour into the stratosphere (Millán et al., 2022; Sellitto et al., 2022). Jenkins et al. (2023) determined the HTHH eruption increased volcanic ERF by $+0.12 \text{ W m}^{-2}$ due to sWV. The 2022 volcanic ERF has therefore been increased to account for this. sWV injections from other volcanic eruptions historically have been assumed to be negligible. This assumption for the whole Holocene is probably incorrect (1883 Krakatau may have also emitted substantial amounts of sWV

(Joshi and Jones, 2009)), but at present no known proxy datasets for sWV injections from volcanic eruptions before the
180 observational era exist. After 1991 Pinatubo there was a marked increase in sWV above Colorado (40°N) that peaked and
declined over a period of around three years following the eruption (Hurst et al., 2011). However, this was significantly smaller
than the perturbation from HTHH (Millán et al., 2022), may be obscured against a background of increasing sWV from a
changing QBO state (Fueglistaler and Haynes, 2005), and reanalysis data shows no obvious water vapour signal averaged
185 across the tropical lower stratosphere (Dessler et al., 2014). We therefore do not adjust the volcanic ERF for sWV from 1991
Pinatubo or any other eruption.

S5. Earth energy imbalance

While changes in EEI have been effectively monitored at the top of the atmosphere by satellites since the mid-2000s, we rely
on estimates of OHC change to determine the absolute magnitude of EEI and its evolution on inter-annual to multi-decadal
190 time series. The AR6 assessment of ocean heat content change for the 0–2000 m layer was based on global annual mean time
series from five ocean heat content datasets: IAP (Cheng et al., 2017), Domingues et al. (2008), EN4 (Good et al., 2013), Ishii
et al. (2017) and NCEI (Levitus et al., 2012). Four of these datasets routinely provide updated OHC time series for the BAMS
State of the Climate report, and all are used for the GCOS Earth heat inventory (von Schuckmann et al., 2020, 2023a) and the
annual WMO global state of the climate. The uncertainty assessment for the 0–2000 m layer used the ensemble method
195 described by Palmer et al. (2021) that separately accounts for parametric and structural uncertainty. The OHC change >2000 m
and associated uncertainty were assessed based on trend analysis of the available hydrographic data following Purkey and
Johnson (2010). All five of the datasets used for the 0–2000 m OHC assessment are now updated at least annually and should
in principle support an AR6 assessment time series update within the first few months of each year. There is potential to
increase the observational ensemble used in the assessment by supplementing this set with additional data products that are
200 also available annually for future updates. A full propagation of uncertainties across all heat inventory components depends
on the specific choice of time period, and different estimates are not directly comparable. Therefore, we take a simple pragmatic
approach, using the total ocean heat content uncertainty as a proxy for the total uncertainty, since this term is 2 orders of
magnitude larger than the other terms (Forster et al., 2021). To provide estimates of the EEI up to the year 2023, we scale up
the values of OHC change in 2021, 2022 and 2023 to reflect the 91 % contribution of the ocean to changes in the Earth heat
205 inventory. The EEI is then simply computed as the difference in global energy inventory over each period, converted to units
of watts per square metre (W m^{-2}) using the surface area of the Earth and the elapsed time. The uncertainties in the global
energy inventory for the end-point years are assumed to be independent and added in quadrature, following the approach used
in AR6 (Forster et al., 2021). Estimates of EEI should also account for the other elements of the Earth heat inventory, i.e. the

atmospheric warming, the latent heat of global ice loss and heating of the continental land surface (Forster et al., 2021; Cuesta-
210 Valero et al., 2021, 2023a; Steiner et al., 2020; Nitzbon et al., 2022a; Vanderkelen et al., 2020; Adusumilli et al., 2022). Some
of these components of the Earth heat inventory are routinely updated by a community-based initiative reported in von
Schuckmann et al. (2020, 2023a). However, in the absence of annual updates to all heat inventory components, a pragmatic
approach is to use recent OHC change as a proxy for EEI, scaling the value up as required based on historical partitioning
between Earth system components.

215 **S6. Global surface temperature**

Surface temperature information on land and sea is available with low latency through WMO distribution channels, with
monthly station data from a substantial number of stations reported within a few days of the end of the month. Sea-surface
temperature data from ships and buoys are gathered from the Global Telecommunication System with a short delay. These are
consolidated into global data sets by a number of institutions, making it feasible to report GMST updates within a few weeks
220 of the end of the period of interest. The number of reporting locations on land with near-real time data available for reporting
for the most recent periods is typically less than that available for historical data, as not all observation sites report recent data
reliably, but this lower observation density only slightly increases the uncertainty in estimates of recent annual GMST
compared with the past 20-30 years (Trewin et al., 2021).

225 The GMST assessment in AR6 was largely based on four datasets: HadCRUT5 (Morice et al., 2021), Berkeley Earth (Rohde
and Hausfather, 2020), NOAAGlobalTemp - Interim (Vose et al., 2021) and Kadow et al. (2020). The four GMST datasets
were chosen by virtue of being quasi globally complete, having data back to 1850, using the most recent generation of SST
analyses and using analysed (rather than climatological) values over sea ice. The first two of these are routinely updated
operationally, with data for each year becoming available in the first few weeks of the following year. NOAAGlobalTemp -
230 Interim was not updated operationally at the time AR6 was published but became NOAA's main operational GMST dataset
(under the name NOAAGlobalTemp 5.1) as of January 2023. All three datasets are updated and published monthly. The dataset
by Kadow et al. is updated on an ad hoc basis by the authors. A fifth data set, China - Mean Surface Temperature (China-
MST) (Sun et al., 2021), which meets all the GMST dataset criteria except for treatment of sea ice areas, is used both in AR6
and here for global temperatures over land areas only. Although the version of the Kadow et al. (2020) dataset reported in that
235 paper used HadCRUT4 as its base, the version used in AR6 and subsequently used HadCRUT5 as its base.

In the last year, there has been a significant version change to NOAAGlobalTemp (now version 6.0.0). This uses a new artificial
neural network approach to reconstruct temperatures over land (Huang et al., 2022) in place of the empirical orthogonal

teleconnection approach used in version 5.1. This change has little impact on long-term trends at global scale since the low-
240 frequency component in the land surface air temperature (LSAT) reconstruction has not changed, but has a substantial impact
on spatial and short-term temporal variability. Version 6.0.0 shows approximately 0.01 °C less warming from 1850-1900 to
recent time periods (such as 2013-2022) than version 5.1, principally due to differences in the early part of the 1850-1900
baseline period.

245 To date, all four GMST datasets remain supported, and those version changes which have occurred since AR6 have not had a
material impact on long-term temperature changes, but it is likely that more substantive version changes will occur to one or
more over time, potentially leading to differences from the AR6. Version changes to date since AR6 have resulted in the
warming from 1850-1900 to 2011-2020, 2010-2019 and 2001-2020 each being 0.01 °C greater in the most recent dataset
versions than that reported in AR6.

250

The key differences between the AR6 datasets and those used in the annual WMO and BAMS State of the Climate reports are
that WMO and BAMS also incorporate reanalyses (ERA5 and JRA-55, expected to be superseded by JRA-3Q during 2024).
These reports also include the GISTEMP (Lenssen et al., 2019) dataset (excluded by AR6 because it starts in 1880) but do not
include the dataset by Kadow et al. (as that is not updated operationally).

255

The GMST values used in AR6 were calculated from the gridded data sets produced by the data providers, using a consistent
methodology - calculating the mean anomaly for each of the northern and southern hemisphere as a latitude-weighted mean of
available gridpoint values, then defining the global mean anomaly as the mean of the two hemispheric values. (This is
equivalent to the method used by the Met Office Hadley Centre to report global values from HadCRUT5). The values thus
260 calculated may differ from those reported by the data providers themselves, due to different averaging methodologies.
Although the difference is less pronounced in the AR6 datasets than in earlier generations of datasets, there are more gridpoints
with missing data in the Southern Hemisphere than the Northern (particularly before an observation network was established
on Antarctica in the 1950s), and using hemispheric means ensures that the two hemispheres are equally weighted.

265 The uncertainty assessment in AR6 combines the spread of the individual datasets with uncertainties derived from ensembles
for HadCRUT5 and an earlier version of NOAA GlobalTemp, with the other two datasets assumed to have the same uncertainty
as HadCRUT5. HadCRUT5 is the only one of the datasets for which regularly updated ensembles are currently produced,
limiting the extent to which uncertainty assessments can be regularly updated from those used in AR6. In this update it was
assumed that the width of the confidence interval for each individual dataset was the same as that used in AR6.

270 **S7 Human-induced global warming**

S7.1 Estimates of global surface temperature: GMST and GSAT in attributed warming assessments

AR6 WGI (Chap. 2 Cross-Chap. Box 2.3, Gulev et al., 2021) described how global mean surface air temperature (GSAT), as is typically diagnosed from climate models, is physically distinct from the global mean surface temperature (GMST) estimated from observations, which generally combine measurements of near-surface temperature over land and in some cases over ice, with measurements of sea surface temperature over the ocean. Gulev et al. (2021) assessed with high confidence that long-term trends in the two indicators differ by less than 10 %. However, based on conflicting lines of evidence from climate models and direct observations, the former showing stronger warming of GSAT compared to GMST, the latter tending to show the opposite, there is low confidence in the sign of the difference in trends. Therefore, with medium confidence, in AR6 WGI Chap. 3 (Eyring et al., 2021), the best estimates and likely ranges for attributable warming expressed in terms of GMST were assessed to be equal to those for GSAT, which means that the AR6 attributable warming assessment does not distinguish between GMST and GSAT. As such, while WGI Chap. 3 (Eyring et al., 2021) treated estimates of attributable warming in GSAT and GMST from the literature together without any rescaling, we note that climate-model-based estimates of attributable warming in GSAT are expected to be systematically higher than corresponding estimates of attributable warming in GMST (see e.g. Cowtan et al., 2015; Richardson et al., 2018; Beusch et al., 2020; Gillett et al., 2021). Therefore, given an opportunity to update these analyses from AR6, it is more consistent and more comparable with observations of GMST to report attributable changes in GMST using all three methods (described in Supplement Sect. S7.2). The SR1.5 assessment of attributable warming was given in terms of GMST, which is continued here. Therefore, in line with Sect. 6, AR6 WGI, and SR1.5, we adopt GMST as the estimate of global surface temperature. Findings are presented in Figs. S3, S4 and S5 and Tables S3 and S4.

S7.2 Methods to estimate human-induced warming

Both SR1.5 and AR6 drew on evidence from a range of literature for their assessments of human-induced warming, before selecting results from a smaller subset to produce a quantified estimate. While both the SR1.5 and AR6 assessments used the latest Global Warming Index (GWI) results (Haustein et al., 2017), AR6 also incorporated results from two other methods, regularised optimal fingerprinting (ROF) (as in Gillett et al., 2021) and kriging for climate change (KCC) (as in Ribes et al., 2021). In AR6, all three methods gave results consistent not only with each other but also results from AR6 WGI Chap. 7 (see WGI Chap. 7 Supplementary Material (Smith et al., 2021b), Fig. 3.8 of AR6 WGI Chap. 3 (Eyring et al., 2021), and Figs. S3, S4 and S5). Note that the results from Chap. 7 were not included in the AR6 WGI final calculation because they were not statistically independent of other methods. Of the methods used, two (Gillett et al., 2021; Ribes et al., 2021) relied on CMIP6 DAMIP (Gillett et al., 2016) simulations which ended in 2020 and hence require modifications to update to the most recent years. The other two methods (Haustein et al., 2017; Smith et al., 2021b) are fully updatable and can also be made consistent

300 with other aspects of the AR6 assessment and methods. The three methods used in the final assessment of contributions to
warming in AR6 are used again with revisions for this annual update and are presented here along with any updates to their
approaches.

S7.2.1 Global Warming Index

Introduced in Otto et al. 2015, and refined with full uncertainty assessment in Hausteine et al., 2017, the Global Warming Index
305 (GWI) quantifies anthropogenic warming by using an established “multi-fingerprinting” approach to decompose total warming
into its various components; preliminary anthropogenic and natural warming time series are first estimated from radiative
forcings, and a multivariate linear regression is then taken between these preliminary GMST contributions and observed
GMST, with the best fit providing the attributed anthropogenic and natural contributions to warming. As such, the GWI
attribution method is directly tied to observations and therefore the resulting central estimate for human-induced warming has
310 a relatively small dependence on the size of the uncertainties in climate sensitivity and forcing.

Substantive annual updates to the GWI assessment depend on annual updates for effective radiative forcings (ERFs) and
observed temperature (GMST), both of which are provided as a part of this update (Sects. 4 and 6 respectively). The remaining
inputs to the GWI assessment are updated at the less-frequent CMIP cadence; however, these contributions only weakly
315 influence the GWI results. Further, by recomputing a “historical-only” GWI time series based only on data up to a given year,
it can be shown that GWI is relatively insensitive to end-date or short-term fluctuations in observed GMST, minimising
potential confusion about the current level of warming, such as the perception of a hiatus or acceleration (see AR6 WGI
Chapter 3 Cross-Chapter Box 3.1, Eyring et al., 2021), due to short-term internal variability. This, combined with the
conceptual simplicity of the method, makes the GWI a relatively transparent and robust method for attributing anthropogenic
320 warming and well-suited to providing reliable annual updates.

Where the GWI method previously separated warming contributions into two components, “anthropogenic” and “natural”, and
independently attributed them, this update further separates and independently attributes contributions within the
Anthropogenic component, adopting the groupings from AR6: “well-mixed greenhouse gases”, “other human forcings” and
325 “natural forcings”. The climate response model used to estimate (pre-regression) warming from radiative forcing is updated
from the AR5 Impulse Response model (AR5-IR; from AR5 Chapter 8 Supplement (Myhre et al., 2013b)) used in Hausteine et
al. (2017) to the Finite-amplitude Impulse Response model (FaIR; Leach et al., 2021; Smith et al., 2018b; Millar et al., 2017),
which has established use in SR1.5 and AR6; climate response uncertainty is included by using around 30 sets of parameters
that correspond to FaIR emulating the CMIP6 ensemble, as provided in Leach et al. (2021). The updated historical ERF input
330 to FaIR is given in Sect. 4, with uncertainty accounted for using a representative 1000-member probabilistic ensemble.

Observed GMST and its uncertainty are provided by the 200-member ensemble of the annually updated HadCRUT5 (Morice et al. 2021; see Sect. 6). Uncertainty from internal variability is accounted for by using between 100-200 realisations of internal variability sampled from the CMIP6 piControl simulations (Nicholls et al., 2021). Since some CMIP6 models may have unrealistically high decadal variability, our estimates of uncertainty may be conservative (Erying et al., 2021). Here, to partly address this, piControl timeseries are first filtered, removing simulations that drift by more than 0.15 °C per decade or exhibit unrealistic variability amplitudes. The parameters for FaIR (given in Leach et al., 2021) are tuned to GSAT outputs from CMIP6; the outputs from FaIR are not rescaled to account for the difference between GSAT and GMST in the tuning since any rescaling would be immediately and completely regressed out in the next step of the attribution process; this lack of rescaling is additionally broadly consistent with the AR6 assessment which concluded with medium confidence that GSAT and GMST are representative of each other – see Supplement Sect. S7.1. In future, FaIR could be re-tuned to GMST estimates from CMIP6 in addition to GSAT outputs to examine potential differences in the response that cannot be accounted for through a linear rescaling, though differences in the final attribution results from such a study are expected to be minimal; the regression onto HadCRUT5 provides the strongest constraint.

Producing the GWI ensemble with ~1 billion members is computationally expensive; therefore an ensemble with ~6 million members is randomly subsampled to obtain results. Uncertainty converges at this scale, and repeat random samplings at the same scale lead to variation in the results of on the order of 0.01°C.

Compared to Forster et al. 2023, the GWI calculation remains the same, differing only by (i) using ERFs and observed temperatures updated to 2023, and (ii) averaging results across five random ~6 million member sub-samplings instead of one in order to maximise robustness

S7.2.2 Kriging for climate change

The kriging for climate change method was originally introduced by Ribes et al. (2021), and subsequently extended in Qasmi and Ribes (2022), to attribute past warming and constrain temperature projections over the 21st century. This statistical method is very similar to ensemble Kalman filtering or kriging. In the original publication (Ribes et al., 2021), a subset of 22 CMIP6 models was considered. For each of them, a statistical procedure was applied to estimate the warming induced by GHG, ANT (temporal smoothing procedure) or NAT (using an Energy Balance Model) forcings, respectively. This subset of models was subsequently used to form an a priori distribution (in a Bayesian sense) of past attributable warming. Then the posterior distribution of past attributable warming given observations was derived. This application was based on HadCRUT4-CW GMST observations (Cowtan and Way, 2014), inflated by 6% to account for stronger warming of GSAT relative to GMST.

Results from this calculation were quoted in Eyring et al. (2021). The update made here uses the same subset of 22 CMIP6 models. However, HadCRUT5 observations are used, instead of previous datasets, over an extended 1850-2022 period. Consistent with the AR6 assessment about GMST to GSAT warming ratio, no scaling correction is applied; i.e. the global mean value from HadCRUT5 is assumed to be representative of GSAT changes (see Sect. S7.1). As it relies on available CMIP6 simulations, this update assumes that the world has followed a SSP2-4.5 pathway since 2015. Emissions in the SSP scenarios are similar in the period up until 2023 and close to those which have occurred (e.g. Chen et al., 2021); therefore this is a reasonable approximation. Future updates with this method will incorporate new observations. In parallel, we will try to replace the CMIP6 models by emulators, thus allowing the latest available estimates of radiative forcings to be considered, instead of the SSP2-4.5 scenario.

S7.2.3 Regularized optimal fingerprinting

Optimal fingerprinting is the name given to optimal regression-based approaches to attribution, in which observed anomalies are regressed onto the simulated response to individual forcings from climate models, with the regression coefficients used to infer attributable contributions to observed changes (e.g. Allen and Stott, 2003; Eyring et al., 2021). Ribes et al. (2013) proposed an improved version of the standard total least squares regression, known as regularised optimal fingerprinting, which exhibited improved accuracy in perfect model tests. Gillett et al. (2021) applied this approach to regress observed 5-year mean observed GMST onto the simulated response to individual forcings from the DAMIP simulations (Gillett et al., 2016) of 13 CMIP6 models. In order to ensure a like-for-like comparison, Gillett et al. (2021) regressed observations of GMST, derived from gridded non-infilled near-surface air temperature over land and sea ice, and sea surface temperature over oceans, onto GMST derived from CMIP6 model output in the same way (Cowtan et al., 2015). However, since globally complete GSAT is usually used in the climate impact literature which served as a basis for global warming goals, Gillett et al. (2021) used regression coefficients to infer attributable warming in globally complete GSAT.

Gillett et al. (2021) used CMIP6 DAMIP simulations which generally finished in 2020 and therefore cannot directly be used to infer attributable warming in subsequent years. However, some modelling centres ran single-forcing DAMIP simulations into the future under the SSP2-4.5 scenario (Gillett et al., 2016). Data from concatenated historical and ssp245, hist-nat and ssp245-nat, and hist-GHG and ssp245-GHG were taken from CanESM5 (50, 10, 10), IPSL-CM6A-LR (11, 10, 6) and MIROC6 (3, 50, 50), where numbers in brackets indicate the respective ensemble sizes. Our approach assumes that observed drivers have evolved as in the SSP2-4.5 scenario over the period since 2015, which is a reasonable assumption to the present (e.g. Chen et al., 2021). As in Gillett et al. (2021), internal variability was estimated from intra-ensemble anomalies. Whereas the Gillett et al. (2021) results assessed by Eyring et al. (2021) were based on HadCRUT4, this dataset is no longer being updated, and therefore we use the non-infilled version of HadCRUT5 here (Morice et al., 2021). As shown by Gillett et al.

(2021), using HadCRUT5 in place of HadCRUT4 results in a 7% increase in the best estimate of anthropogenic warming for 2010-2019. Gillett et al. (2021) regressed 34 5-year means of GMST over the period 1850-2019 onto simulated GMST over the same period. Here we extend the analysis using 35 5-year means, with the latter based on observations from January 2020 to February 2023 and the model output masked in the same way. In order to be consistent with the Global Warming Index and kriging for climate change approaches described above, and for comparison with GMST observations, we primarily report attributable warming in globally complete GMST here, rather than GSAT (see Sect. S7.1). Calculated anthropogenic warming in GSAT in 2010-2019 computed using HadCRUT5 with this approach of 1.16 (1.04-1.29) °C can be compared with the same quantity reported in Gillett et al. (2021) (their Supplementary Table 1) of 1.18 (1.09-1.27) °C, indicating good consistency.

The method described above is easily updatable into the future using the same set of simulations, simply by updating observations to a later date and masking model output accordingly. As in the KCC method, a caveat to this approach is that it relies on SSP2-4.5 simulations from which actual anthropogenic forcing might be expected to gradually diverge and from which actual natural forcing could rapidly diverge, for example, were a major volcanic eruption to occur.

Table S3 Estimates of global mean surface air temperature (GSAT) warming attributable to multiple influences (in °C) relative to the 1850–1900 baseline period. Values are given as the median, with the 5-95 percentile range in brackets, provided to 0.01°C precision. GSAT results here are only provided for regularised optimal fingerprinting (ROF) because the GSAT results for the other attribution methods (the Global Warming Index (GWI) and kriging for climate change (KCC)) are identical to the GMST results for those methods.

variable	2010-2019 (decade average)	2014-2023 (decade average)	2017 (trend-based)	2023 (trend-based)
<i>Human-induced</i>	1.18 [1.05 to 1.31]	1.30 [1.15 to 1.45]	1.22 [1.08 to 0.36]	1.45 [1.28 to 1.63]
<i>Well-mixed greenhouse gases</i>	1.44 [1.22 to 1.67]	1.55 [1.31 to 1.79]	1.49 [1.26 to 1.73]	1.67 [1.41 to 1.93]
<i>Other human forcings</i>	-0.25 [-0.45 to -0.05]	-0.25 [-0.45 to -0.05]	-0.26 [-0.47 to - 0.05]	-0.23 [-0.43 to -0.04]
<i>Natural</i>	0.02 [-0.02 to 0.06]	0.01 [-0.03 to 0.05]	0.02 [-0.02 to 0.05]	0.01 [-0.04 to 0.06]

S7.3 Results from each Attribution Method

Results for each attribution method, including headline results and timeseries, are available in csv form in the Climate Indicator repository: <https://github.com/ClimateIndicator/anthropogenic-warming-assessment/>.

415

Table S4 Estimates of global mean surface temperature (GMST) warming attributable to multiple influences (in °C) relative to the 1850–1900 baseline period, provided for each warming attribution method and the overall multi-method assessment. Values for individual attribution methods are given as the median, with the 5-95 percentile range in brackets, provided to 0.01 °C precision. Values for the assessment are calculated as defined in Sect. S7.4 and given as best estimates with likely ranges in brackets.

420

Variable	Method	2010-2019 (decade average)	2014-2023 (decade average)	2017 (single year)	2023 (single year)	2017 (trend- based)	2023 (trend- based)
<i>Human-induced</i>	<i>GW</i>	1.09 [0.98 to 1.18]	1.18 [1.07 to 1.28]	1.15 [1.03 to 1.25]	1.29 [1.16 to 1.40]	1.13 [1.02 to 1.23]	1.29 [1.16 to 1.40]
	<i>KCC</i>	1.05 [0.91 to 1.17]	1.15 [1.00 to 1.29]	1.11 [0.96 to 1.24]	1.26 [1.10 to 1.42]	1.10 [0.96 to 1.24]	1.26 [1.10 to 1.42]
	<i>ROF</i>	1.12 [0.99 to 1.25]	1.24 [1.09 to 1.38]	1.19 [1.04 to 1.35]	1.39 [1.16 to 1.61]	1.16 [1.03 to 1.29]	1.38 [1.21 to 1.55]
	<i>Assessment</i>	1.09 [0.9 to 1.3]	1.19 [1.0 to 1.4]	1.15 [0.9 to 1.4]	1.31 [1.1 to 1.7]	1.13 [0.9 to 1.3]	1.31 [1.1 to 1.6]
<i>Well-mixed greenhouse gases</i>	<i>GW</i>	1.28 [1.02 to 1.56]	1.36 [1.09 to 1.66]	1.33 [1.06 to 1.62]	1.45 [1.16 to 1.77]	1.32 [1.06 to 1.61]	1.45 [1.16 to 1.76]
	<i>KCC</i>	1.46 [1.13 to 1.77]	1.55 [1.19 to 1.88]	1.52 [1.17 to 1.84]	1.65 [1.27 to 2.01]	1.52 [1.17 to 1.84]	1.65 [1.27 to 2.01]
	<i>ROF</i>	1.39 [1.17 to 1.60]	1.49 [1.26 to 1.72]	1.45 [1.21 to 1.68]	1.60 [1.35 to 1.86]	1.43 [1.21 to 1.66]	1.60 [1.35 to 1.85]
	<i>Assessment</i>	1.38 [1.0 to 1.8]	1.47 [1.0 to 1.9]	1.43 [1.0 to 1.9]	1.57 [1.1 to 2.1]	1.42 [1.0 to 1.9]	1.57 [1.1 to 2.1]
<i>Other human forcings</i>	<i>GW</i>	-0.19 [-0.46 to 0.05]	-0.18 [-0.45 to 0.06]	-0.18 [-0.45 to 0.06]	-0.16 [-0.45 to 0.08]	-0.19 [-0.47 to 0.06]	-0.16 [-0.44 to 0.09]
	<i>KCC</i>	-0.41 [-0.70 to -0.12]	-0.40 [-0.70 to -0.10]	-0.41 [-0.70 to -0.11]	-0.39 [-0.70 to -0.07]	-0.41 [-0.71 to -0.11]	-0.39 [-0.70 to -0.08]

	<i>ROF</i>	-0.24 [-0.44 to -0.05]	-0.24 [-0.44 to -0.05]	-0.24 [-0.45 to -0.04]	-0.23 [-0.44 to -0.01]	-0.25 [-0.46 to -0.05]	-0.23 [-0.42 to -0.04]
	<i>Assessment</i>	-0.28 [-0.7 to 0.1]	-0.27 [-0.7 to 0.1]	-0.28 [-0.7 to 0.1]	-0.26 [-0.7 to 0.1]	-0.28 [-0.8 to 0.1]	-0.26 [-0.7 to 0.1]
<i>Natural</i>	<i>GWI</i>	0.06 [0.03 to 0.11]	0.06 [0.03 to 0.11]	0.06 [0.03 to 0.11]	0.06 [0.03 to 0.11]	0.06 [0.03 to 0.11]	0.06 [0.02 to 0.11]
	<i>KCC</i>	0.06 [0.04 to 0.08]	0.05 [0.04 to 0.07]	0.06 [0.04 to 0.08]	0.04 [0.03 to 0.06]	0.06 [0.04 to 0.08]	0.05 [0.03 to 0.06]
	<i>ROF</i>	0.02 [-0.02 to 0.05]	0.01 [-0.02 to 0.05]	0.01 [-0.03 to 0.06]	0.01 [-0.05 to 0.06]	0.02 [-0.02 to 0.05]	0.01 [-0.04 to 0.05]
	<i>Assessment</i>	0.05 [-0.1 to 0.2]	0.04 [-0.1 to 0.2]	0.04 [-0.1 to 0.2]	0.04 [-0.1 to 0.2]	0.05 [-0.1 to 0.2]	0.04 [-0.1 to 0.2]

Validation of updated lines of evidence for assessing contributions to observed warming

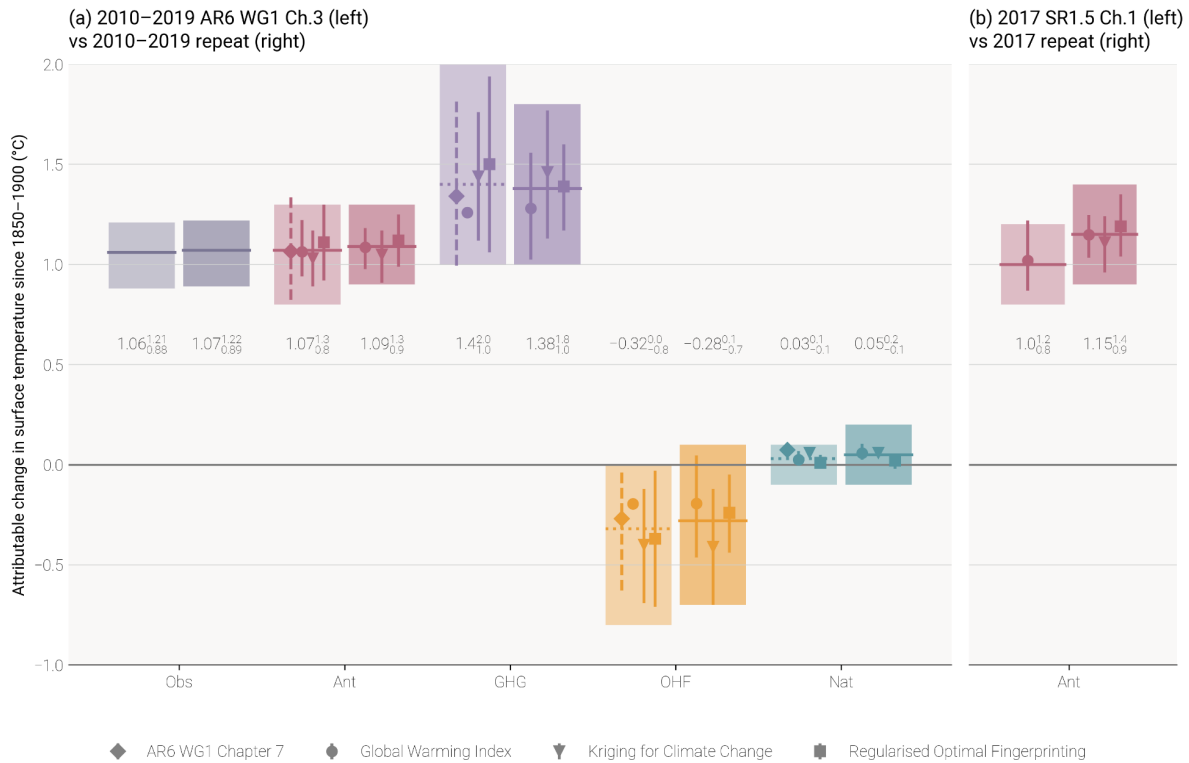
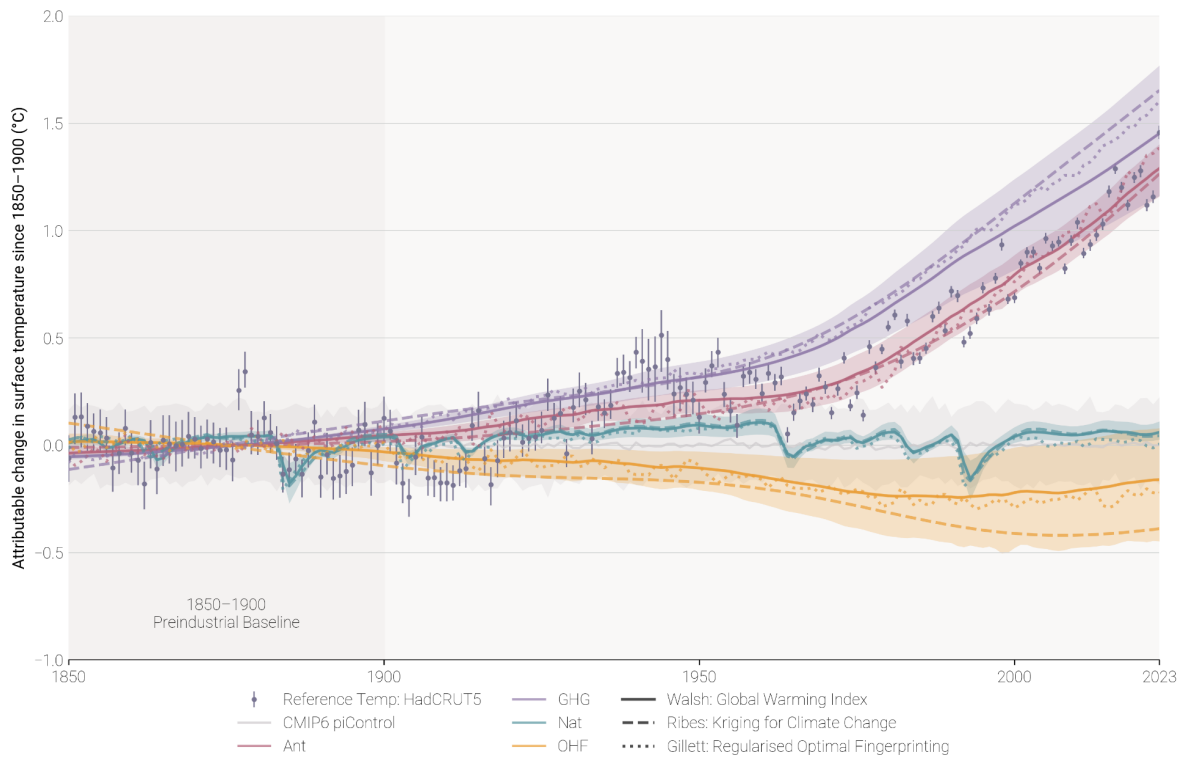


Figure S3 Assessed contributions to observed warming and supporting lines of evidence; see AR6 WG1 Fig. 3.8. The shaded bands show the assessed *likely* ranges of temperature change, relative to the 1850-1900 baseline, attributable to total anthropogenic

425 influence (Ant), well-mixed greenhouse gases (GHGs), other human forcings (OHFs), and natural forcings (Nat). The left of each pair of bands depicts the results quoted from AR6, and the right of each pair of bands depicts a repeat calculation for the same period as the IPCC assessment, using the revised datasets and methods, to validate the updated assessment of attributable warming. Panel (a) presents decade-average warming as used in AR6, with results quoted from AR6 WGI Chapter 3 on the left and the repeat assessment on the right. The solid horizontal bar in each band shows the best estimate for each warming component; if no best estimate was provided, it was retrospectively calculated using the AR6 method and depicted using a horizontal dotted line to facilitate comparison. In AR6, Global Warming Index results were reported as GMST, kriging for climate change results were calculated as GMST and scaled by 1.06 for reporting as GSAT, and regularised optimal fingerprinting was reported as GSAT; for the repeat, all methods are reported in terms of GMST (see Sect. S7.1 for discussion). Panel (b) presents single-year warming as used in SR1.5, with results quoted from SR1.5 Chapter 1 on the left (which was based only on the Global Warming Index) and the repeat assessment on the right, which now includes all of the attribution methods and the multi-method assessment approach used in AR6, as discussed in Sect. S7.4. Both bars are reported in GMST. No assessment was provided for components other than Ant in SR1.5.

Timeseries for each attribution method used in the assessment of contributions to observed warming



440 **Figure S4** Time series for each attribution method used in the updated assessment of warming contributions, expressed in terms of global mean surface temperature (GMST). Coloured plumes correspond to warming contributions broken down by natural forcings (Nat), well-mixed greenhouse gases (GHGs) and other human forcings (OHFs). Total human-induced warming (Ant) is therefore the sum of contributions from GHG and OHF. The plume range is given by the 5-95% range of the Global Warming Index (GWI), with the GWI best estimate given by the solid lines. The dashed line presents the best estimate from the kriging for climate change (KCC) method, and the dotted line presents the best estimate from the regularised optimal fingerprinting (ROF) method. GWI and KCC are given as annual values based on infilled GMST from HadCRUT5; ROF is given as annual values of globally complete GMST. The CMIP6 pre-industrial control (piControl) simulations are used as a proxy for multiple samplings of internal variability and are used to account for attribution uncertainty resulting from internal variability in the GWI method (see Sect. S7.2.1).

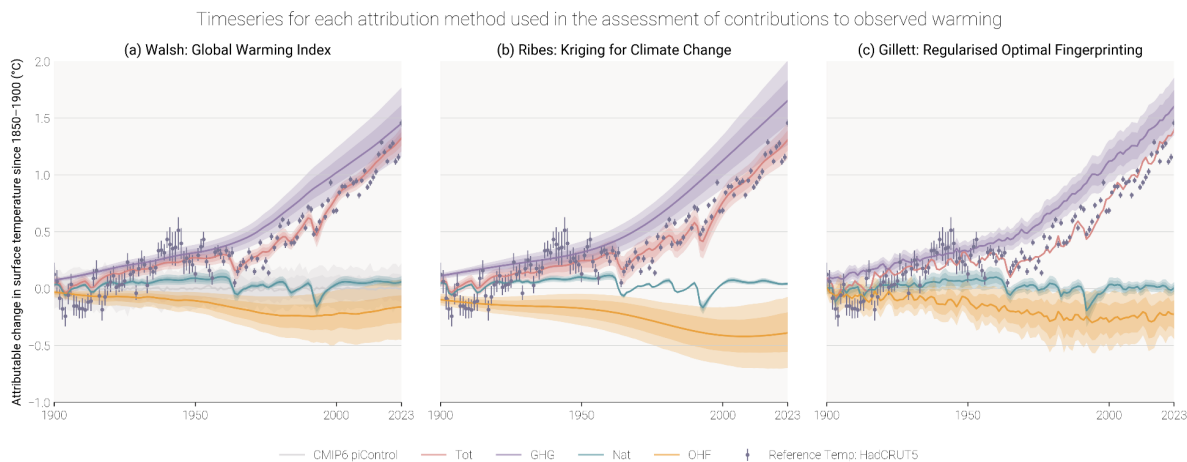


Figure S5 Time series for each attribution method used in the updated assessment of warming contributions, expressed in terms of global mean surface temperature (GMST). Coloured plumes are given for both 17-83% and 5-95% ranges and correspond to warming contributions to observed warming broken down by natural forcings (Nat), well-mixed greenhouse gases (GHGs) and other human forcings (OHFs). Total warming (Tot) is the total attributable warming and therefore the sum of contributions from GHG, OHF and Nat. Observation data from (infilled) HadCRUT5 are presented with 9-95% uncertainty bars. Panel (a) presents results from the Global Warming Index method (Sect. S7.2.1); the CMIP6 pre-industrial control (piControl) simulations are used as a proxy for multiple samplings of internal variability and used to account for uncertainty in the attribution resulting from internal variability (see Sect. S7.2.1). Panel (b) presents results from the kriging for climate change methods (Sect. S7.2.2). Panel (c) presents results from regularised optimal fingerprinting (Sect. S7.2.3), with the time series for Tot being approximated by the sum of the Ant and Nat medians; note that this is different from GWI and KCC, where Tot is a directly attributed quantity.

S7.4 Updated IPCC assessment approach of attributed global warming

S7.4.1 Updated estimate using the AR6 WGI methodology

Factoring in results from each of the three attribution methods (see Sect. S7.2), AR6 WGI Chap. 3 (Eyring et al., 2021) defined the *likely* range for each warming component as the smallest 0.1 °C precision range that enveloped the 5th to 95th percentile ranges of each method. In addition, a best estimate was provided for the human-induced (Ant) warming component, calculated as the mean of the 50th percentile values for each method. Best estimates were not provided in AR6 for the other components (well-mixed greenhouse gases (GHGs), other human forcings (OHFs) and natural forcings (Nat)), with their values in AR6 WGI Fig. SPM.2(b) simply being given as the midpoint between the lower and upper bound of the *likely* range and therefore not directly comparable with the central values given for human-induced and observed warming. In order to make a meaningful and consistent comparison, and provide insight into interannual changes, an improvement is made in this update: the multi-method-mean best-estimate approach is extended for all warming components.

Note that in IPCC assessments, *likely* statements typically correspond to 66 – 100% probability, whereas *very likely* statements correspond to 90 – 100% probability. Despite deriving the overall multi-method uncertainty ranges from the 5-95th percentile

ranges for each method, the overall uncertainty was conservatively assessed in AR6 to be *likely* rather than *very likely*, which noted that the methods may “underestimate the importance of the structural limitations of climate models, which probably do not represent all possible sources of internal variability; use too simple climate models, which may underestimate the role of internal variability; or underestimate model uncertainty, especially when using model ensembles of limited size and inter-
475 dependent models, for example through common errors in forcings across models” (Eyring et al., 2021). We maintain this choice of *likely* in these updates. The *likely* confidence of the AR6 assessment is also consistent with the *likely* confidence given in SR1.5 assessment - see Supplement Sect. S7.4.2.

S7.4.2 Updated estimate using the SR1.5 methodology applied to the AR6 WGI datasets

480 While a variety of literature was drawn upon for the assessment of human-induced warming in SR1.5 Chap. 1 (Allen et al., 2018), only one method, the Global Warming Index (GWI), was used to provide a quantitative assessment of the 2017, “present-day”, level of human-induced warming. The latest results for this method were provided by Hausteine et al. (2017), who gave a central estimate for human-induced warming in 2017 of 1.01 °C with a 5%–95% range of (0.87 to 1.22 °C). SR1.5 then accounted for methodological uncertainty by rounding this value to 0.1 °C precision for its final assessment of
485 1.0 °C and assessing the 0.8 to 1.2 °C range as a *likely* range. No assessment of the contributions from other components was provided due to limitations in the GWI approach at the time.

While it is possible to continue the SR1.5 assessment approach of using a single method (GWI) rounded to 0.1 °C precision, for the purpose of providing annual updates this is insufficient; (i) 0.1 °C precision is too coarse to capture meaningful inter-
490 annual changes to the level of present-day warming, (ii) using different selections of methods prevents meaningful comparison between the results for decadal mean and present-day warming calculations, and (iii) using the mean of multiple methods increases the robustness of the results. These points are simultaneously addressed in this update by adopting the latest multi-method assessment approach, as established in WGI AR6, for both the AR6 decadal mean warming update and the SR1.5 present-day single-year warming update. Further, where SR1.5 only provided an assessment for human-induced warming,
495 updates in available attribution methods since SR1.5 mean that it is now also possible to provide a fully consistent assessment for all warming components. As with the attribution assessment in SR1.5, this update reports values in Table 6b of the main paper for single-year present-day attributable warming (as discussed in Sect. 7.1), with a comparison to results calculated using the SR1.5 trend-based definition also provided in Sect. 7.3.

S8. Remaining carbon budget

500 Estimating the remaining carbon budget (RCB) requires an estimate of future non-CO₂ warming. The latter estimate is derived from the emissions trajectories as modelled by internally consistent emissions scenarios. While RCB estimates are for CO₂ emissions only, the consideration of non-CO₂ warming implies that assumptions are also made about reductions in other anthropogenic forcings (Rogelj and Lamboll, 2024). These reductions have to be kept in mind, as a shortfall in non-CO₂ greenhouse gas emissions would result in a smaller RCB estimate. For instance, as reported in Rogelj and Lamboll (2024), the

505 estimate of RCBs consistent with limiting warming to 1.5°C assumes a median reduction in CH₄ emissions between 2020 and 2050 of 51% (while the interquartile range across available scenarios is 47–60%), a 22% reduction between 2020 and 2050 in N₂O emissions (interquartile range: 7–35%), and a 78% reduction between 2020 and 2050 in SO₂ emissions (interquartile range: 74–78%). Assumed reductions consistent with other levels of warming are reproduced from Rogelj and Lamboll (2024) and provided in Table S5. The estimates reported in Table 8 of the main paper are based on the median non-CO₂ emission

510 reductions. Falling short of achieving the assumed non-CO₂ greenhouse gas emissions reductions would further reduce the RCB. Sulphur dioxide emissions are more tightly co-controlled with CO₂ reduction because of the phase-out of unabated fossil fuel combustion and air pollution control measures (Rogelj et al., 2014a, 2014b). A shortfall in their reductions would therefore be less conceivable in a net-zero CO₂ world.

515 **Table S5 Non-CO₂ reductions implied in Remaining Carbon Budget (RCB) estimates, adapted from Rogelj and Lamboll (2024). Values represent the changes in non-CO₂ emissions between 2020 and 2050 consistent with the RCB estimates for 1.5°C, 1.7°C and 2.0°C. The median changes are the default and marked in light blue. Any deviation from this median assumption results in an increase or decrease of the RCB estimate.**

Temperature level for which RCB was estimated	Percentile	Implied non-CO ₂ change between 2020 and 2050 [%]		
		CH ₄	N ₂ O	SO ₂
1.5°C	10 th	-69	-47	-80
	25 th	-60	-35	-78
	50 th	-51	-22	-78
	75 th	-47	-7	-74
	90 th	-39	+2	-66
1.7°C	10 th	-62	-42	-78
	25 th	-53	-30	-76

	50 th	-44	-18	-73
	75 th	-39	-3	-68
	90 th	-31	+6	-60
2.0°C	10 th	-51	-35	-75
	25 th	-43	-23	-72
	50 th	-34	-11	-66
	75 th	-27	+2	-59
	90 th	-20	+12	-51

S9. Examples of climate and weather extremes: maximum temperature over land

520 Land average annual maximum temperature (TXx) - Methods

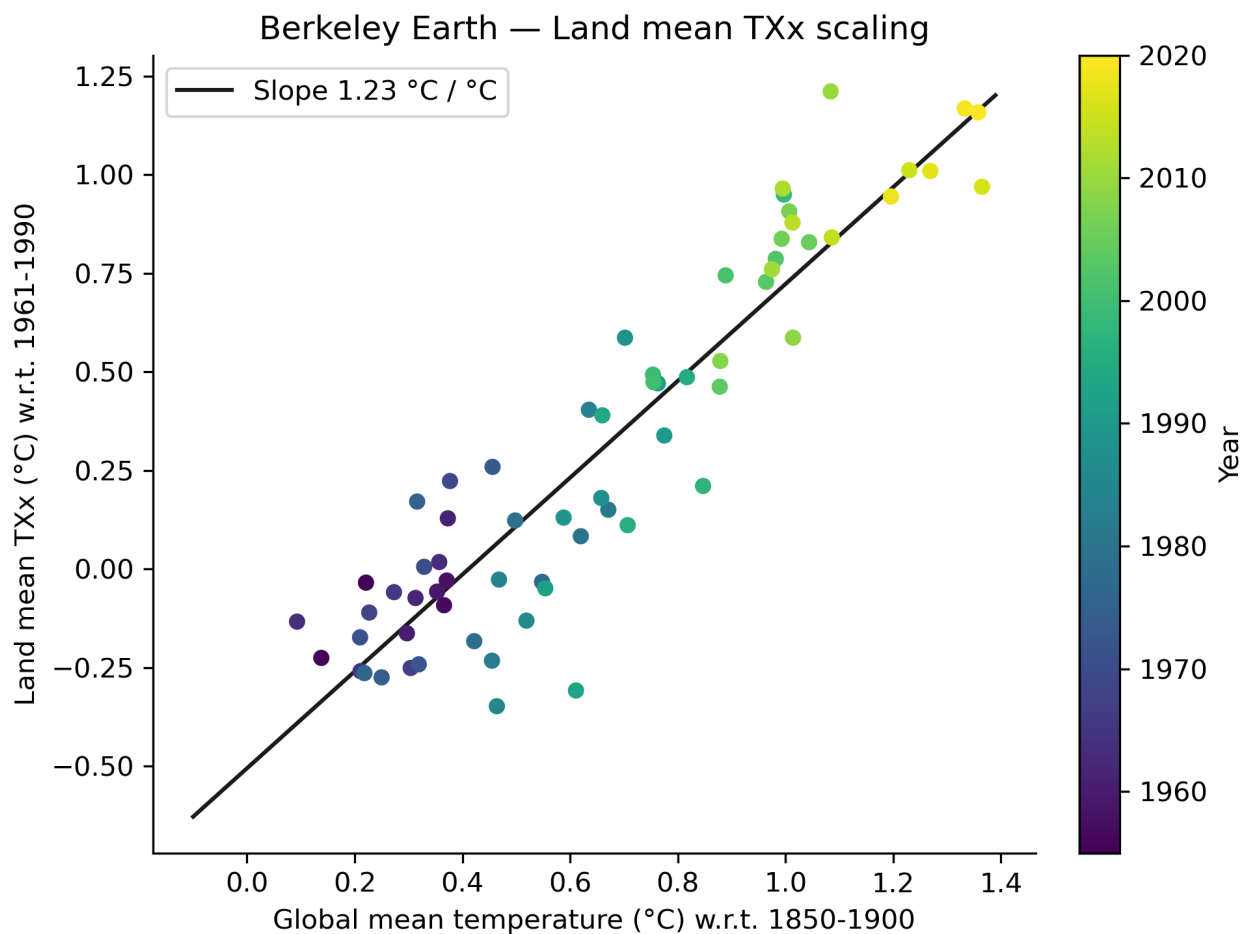
Like the analysis of global mean temperature, the choice of datasets is based on a compromise on the length of the data record, the data availability, near-real-time updates and long-term support. As the indicator (in its current form) averages over all available land grid points, the spatial coverage should be high to obtain a meaningful average, which further limits the choice of datasets. The HadEX3 dataset (Dunn et al., 2020), which is used for Fig. 11.2 in Seneviratne et al. (2021), is static and does not cover years after 2018. We therefore additionally include the Berkeley Earth Surface Temperature dataset (building off Rohde et al., 2013) and the fifth-generation ECMWF atmospheric reanalysis of the global climate (ERA5; Hersbach et al., 2020). Berkeley Earth data currently enable an analysis of annual indices up to 2022, while ERA5 is updated daily with a latency of about 5 d (and the final release occurs after 2–3 months).

For HadEX3, we select the years 1961–2018, to exclude years with insufficient data coverage, and require at least 90 % temporal completeness, thus applying the same criteria as for Fig. 11.2 (Seneviratne et al., 2021). Berkeley Earth provides daily maximum temperatures, and we require more than 99 % data availability for each individual year and grid, such that years with more than 4 missing days are removed. Based on this criterion, Berkeley Earth covers at least 95 % of the global land area from 1955 onwards. ERA5, on the other hand, has full spatio-temporal coverage by design, and hence the entire currently available period of 1950 to 2022 is used. The annual maximum temperature is then computed for each grid cell, and a global area-weighted average is calculated for all grid cells with at least 90 % temporal completeness in the respective available period (1955–2021 and 1961–2018 for Berkeley Earth and HadEX3, while ERA5 is again not affected by this

criterion). We thus enforce high data availability to adequately calculate global land averaged TXx across all three datasets, but their coverage is not identical, which introduces minor deviations in the estimated global land averages. The resulting TXx time series are then computed as anomalies with respect to a baseline period of 1961–1990.

540 Note that the Berkeley Earth daily maximum data has been updated, with changes of several °C for individual grid points and days. These changes partially compensate such that the TXx estimates for individual years differ less than 0.1 °C.

To express the TXx as anomalies with respect to 1850–1900, we add an offset to all three datasets. The offset is based on the Berkeley Earth data and is derived from the linear regression of land mean TXx to the annual mean global mean air temperature
545 over the period 1955 to 2020. The offset is then calculated as the slope of the linear regression times the global mean temperature difference between the reference periods 1850–1900 and 1961–1990 (see Fig. S6). The updated Berkeley Earth data led to a change in offset of 0.01°C compared to Forster et al. (2023).



550

Figure S6 Calculation of land mean annual maximum temperature (TXx) offset between 1850-1900 and 1961-1990. A linear regression of TXx as a function of global mean temperature from Berkeley Earth is fitted to data from 1955-2020. The TXx offset of 0.52 °C is then obtained by multiplying the slope of the linear regression (1.23 °C / °C) with the global mean temperature difference between 1850-1900 and 1961-1990 (0.42°C).

555 References

Adusumilli, S., Straneo, F., Hendricks, S., Korosov, A., Lavergne, T., Lawrence, I., Marzeion, B., Otosaka, I., Schweiger, A., Shepherd, A., Slater, D., Slater, T., Timmermanns, M.-L., and Zemp, M.: GCOS EHI 1960-2020 Cryosphere Heat Content, https://doi.org/10.26050/WDCC/GCOS_EHI_1960-2020_CRHC, 2022.

Allen, M. R. and Stott, P. A.: Estimating signal amplitudes in optimal fingerprinting, part I: theory, *Climate Dynamics*, 21, 477–491, <https://doi.org/10.1007/s00382-003-0313-9>, 2003.

560

- Allen, M. R., O. P. Dube, W. Solecki, F. Aragón-Durand, W. Cramer, S. Humphreys, M. Kainuma, J. Kala, N. Mahowald, Y. Mulugetta, R. Perez, M. Wairiu, and K. Zickfeld, 2018: Framing and Context. In: Global Warming of 1.5°C. An IPCC Special Report on the impacts of global warming of 1.5°C above pre-industrial levels and related global greenhouse gas emission pathways, in the context of strengthening the global response to the threat of climate change, sustainable development, and efforts to eradicate poverty [Masson-Delmotte, V., P. Zhai, H.-O. Pörtner, D. Roberts, J. Skea, P.R. Shukla, A. Pirani, W. Moufouma-Okia, C. Péan, R. Pidcock, S. Connors, J.B.R. Matthews, Y. Chen, X. Zhou, M.I. Gomis, E. Lonnoy, T. Maycock, M. Tignor, and T. Waterfield (eds.)], Cambridge University Press, Cambridge, UK and New York, NY, USA, 49-92, <https://doi.org/10.1017/9781009157940.003>, 2018.
- 565 Beusch, L., Gudmundsson, L., and Seneviratne, S. I.: Emulating Earth system model temperatures with MESMER: from global mean temperature trajectories to grid-point-level realizations on land, *Earth Syst. Dynam.*, 11, 139–159, <https://doi.org/10.5194/esd-11-139-2020>, 2020.
- Chen, D., M. Rojas, B. H. Samset, K. Cobb, A. Diongue Niang, P. Edwards, S. Emori, S. H. Faria, E. Hawkins, P. Hope, P. Huybrechts, M. Meinshausen, S. K. Mustafa, G.-K. Plattner, and A.-M. Tréguier, 2021: Framing, Context, and Methods. In *Climate Change 2021: The Physical Science Basis. Contribution of Working Group I to the Sixth Assessment Report of the Intergovernmental Panel on Climate Change* [Masson-Delmotte, V., P. Zhai, A. Pirani, S. L. Connors, C. Péan, S. Berger, N. Caud, Y. Chen, L. Goldfarb, M. I. Gomis, M. Huang, K. Leitzell, E. Lonnoy, J. B. R. Matthews, T. K. Maycock, T. Waterfield, O. Yelekçi, R. Yu, and B. Zhou (eds.)]. Cambridge University Press, Cambridge, United Kingdom and New York, NY, USA, pp. 147–286, <https://doi.org/10.1017/9781009157896.003>, 2021.
- 575 Cheng, L., Trenberth, K. E., Fasullo, J., Boyer, T., Abraham, J., and Zhu, J.: Improved estimates of ocean heat content from 1960 to 2015, *Sci. Adv.*, 3, e1601545, <https://doi.org/10.1126/sciadv.1601545>, 2017.
- Cowtan, K. and Way, R. G.: Coverage bias in the HadCRUT4 temperature series and its impact on recent temperature trends, *Q.J.R. Meteorol. Soc.*, 140, 1935–1944, <https://doi.org/10.1002/qj.2297>, 2014.
- Cowtan, K., Hausfather, Z., Hawkins, E., Jacobs, P., Mann, M. E., Miller, S. K., Steinman, B. A., Stolpe, M. B., and Way, R. G.: Robust comparison of climate models with observations using blended land air and ocean sea surface temperatures, *Geophys. Res. Lett.*, 42, 6526–6534, <https://doi.org/10.1002/2015GL064888>, 2015.
- 585 Cuesta-Valero, F. J., García-García, A., Beltrami, H., González-Rouco, J. F., and García-Bustamante, E.: Long-term global ground heat flux and continental heat storage from geothermal data, *Clim. Past*, 17, 451–468, <https://doi.org/10.5194/cp-17-451-2021>, 2021.
- Cuesta-Valero, F. J., Beltrami, H., García-García, A., Krinner, G., Langer, M., MacDougall, A. H., Nitzbon, J., Peng, J., von Schuckmann, K., Seneviratne, S. I., Smith, N., Thiery, W., Vanderkelen, I., and Wu, T.: Continental heat storage: Contributions from ground, inland waters, and permafrost thawing, *Earth Syst. Dynam. Discuss.* [preprint], <https://doi.org/10.5194/esd-2022-32>, 2023.
- 590

- Deng, Z., Ciais, P., Tzompa-Sosa, Z. A., Saunio, M., Qiu, C., Tan, C., Sun, T., Ke, P., Cui, Y., Tanaka, K., Lin, X., Thompson, R. L., Tian, H., Yao, Y., Huang, Y., Lauerwald, R., Jain, A. K., Xu, X., Bastos, A., Sitch, S., Palmer, P. I., Lauvaux, T.,
595 d'Aspremont, A., Giron, C., Benoit, A., Poulter, B., Chang, J., Petrescu, A. M. R., Davis, S. J., Liu, Z., Grassi, G., Albergel, C., Tubiello, F. N., Perugini, L., Peters, W., and Chevallier, F.: Comparing national greenhouse gas budgets reported in UNFCCC inventories against atmospheric inversions, *Earth Syst. Sci. Data*, 14, 1639–1675, <https://doi.org/10.5194/essd-14-1639-2022>, 2022.
- Dessler, A. E., Schoeberl, M. R., Wang, T., Davis, S. M., Rosenlof, K. H., and Vernier, J.-P.: Variations of stratospheric water
600 vapor over the past three decades, *J. Geophys. Res.-Atmos.*, 119, 12588-12598, <https://doi.org/10.1002/2014JD021712>, 2014.
- Dhomse, S. S., Mann, G. W., Antuña Marrero, J. C., Shallcross, S. E., Chipperfield, M. P., Carslaw, K. S., Marshall, L., Abraham, N. L., and Johnson, C. E.: Evaluating the simulated radiative forcings, aerosol properties, and stratospheric warmings from the 1963 Mt Agung, 1982 El Chichón, and 1991 Mt Pinatubo volcanic aerosol clouds, *Atmos. Chem. Phys.*, 20, 13627–13654, <https://doi.org/10.5194/acp-20-13627-2020>, 2020.
- 605 Domingues, C. M., Church, J. A., White, N. J., Gleckler, P. J., Wijffels, S. E., Barker, P. M., and Dunn, J. R.: Improved estimates of upper-ocean warming and multi-decadal sea-level rise, *Nature*, 453, 1090–1093, <https://doi.org/10.1038/nature07080>, 2008.
- Dunn, R. J. H., Alexander, L. V., Donat, M. G., Zhang, X., Bador, M., Herold, N., et al. Development of an updated global land in situ-based dataset of temperature and precipitation extremes: HadEX3, *J. Geophys. Res.-Atmos.*, 125, e2019JD032263, <https://doi.org/10.1029/2019JD032263R>, 2020.
- 610 Etminan, M., Myhre, G., Highwood, E. J., and Shine, K. P.: Radiative forcing of carbon dioxide, methane, and nitrous oxide: A significant revision of the methane radiative forcing, *Geophys. Res. Lett.*, 43, 12614-12623, <https://doi.org/10.1002/2016GL071930>, 2016.
- Eyring, V., N. P. Gillett, K.M. Achuta Rao, R. Barimalala, M. Barreiro Parrillo, N. Bellouin, C. Cassou, P. J. Durack, Y.
615 Kosaka, S. McGregor, S. Min, O. Morgenstern, and Y. Sun: Human Influence on the Climate System. In *Climate Change 2021: The Physical Science Basis. Contribution of Working Group I to the Sixth Assessment Report of the Intergovernmental Panel on Climate Change* [Masson-Delmotte, V., P. Zhai, A. Pirani, S.L. Connors, C. Péan, S. Berger, N. Caud, Y. Chen, L. Goldfarb, M.I. Gomis, M. Huang, K. Leitzell, E. Lonnoy, J.B.R. Matthews, T.K. Maycock, T. Waterfield, O. Yelekçi, R. Yu, and B. Zhou (eds.)]. Cambridge University Press, Cambridge, United Kingdom and New York, NY, USA, pp. 423–552, <http://doi:10.1017/9781009157896.005>, 2021.
- 620 Forster, P., T. Storelvmo, K. Armour, W. Collins, J.-L. Dufresne, D. Frame, D.J. Lunt, T. Mauritsen, M.D. Palmer, M. Watanabe, M. Wild, and H. Zhang, 2021: The Earth's Energy Budget, Climate Feedbacks, and Climate Sensitivity. In *Climate Change 2021: The Physical Science Basis. Contribution of Working Group I to the Sixth Assessment Report of the Intergovernmental Panel on Climate Change* [Masson-Delmotte, V., P. Zhai, A. Pirani, S.L. Connors, C. Péan, S. Berger, N.

- 625 Caud, Y. Chen, L. Goldfarb, M.I. Gomis, M. Huang, K. Leitzell, E. Lonnoy, J.B.R. Matthews, T.K. Maycock, T. Waterfield, O. Yelekçi, R. Yu, and B. Zhou (eds.]. Cambridge University Press, Cambridge, United Kingdom and New York, NY, USA, pp. 923–1054, <https://doi.org/10.1017/9781009157896.009>, 2021.
- Forster, P. M., Smith, C. J., Walsh, T., Lamb, W. F., Lamboll, R., Hauser, M., Ribes, A., Rosen, D., Gillett, N., Palmer, M. D., Rogelj, J., von Schuckmann, K., Seneviratne, S. I., Trewin, B., Zhang, X., Allen, M., Andrew, R., Birt, A., Borger, A.,
- 630 Boyer, T., Broersma, J. A., Cheng, L., Dentener, F., Friedlingstein, P., Gutiérrez, J. M., Gütschow, J., Hall, B., Ishii, M., Jenkins, S., Lan, X., Lee, J.-Y., Morice, C., Kadow, C., Kennedy, J., Killick, R., Minx, J. C., Naik, V., Peters, G. P., Pirani, A., Pongratz, J., Schleussner, C.-F., Szopa, S., Thorne, P., Rohde, R., Rojas Corradi, M., Schumacher, D., Vose, R., Zickfeld, K., Masson-Delmotte, V., and Zhai, P.: Indicators of Global Climate Change 2022: annual update of large-scale indicators of the state of the climate system and human influence, *Earth Syst. Sci. Data*, 15, 2295–2327, [https://doi.org/10.5194/essd-15-](https://doi.org/10.5194/essd-15-2295-2023)
- 635 [2295-2023](https://doi.org/10.5194/essd-15-2295-2023), 2023.
- Fueglistaler, S. and Haynes, P. H.: Control of interannual and longer-term variability of stratospheric water vapor, *J. Geophys. Res.*, 110, D24108, <https://doi.org/10.1029/2005JD006019>, 2005.
- Gettelman, A., Christensen, M. A., Diamond, M. S., Gryspeerdt, E., Manshausen, P., Sieir, P., Watson-Parris, D., Yang, M., Yoshioka, M., and Yuan, T.: Has Reducing Ship Emissions Brought Forward Global Warming?, *Geophys. Res. Lett.*, 2024.
- 640 Gillett, N. P., Shiogama, H., Funke, B., Hegerl, G., Knutti, R., Matthes, K., Santer, B. D., Stone, D., and Tebaldi, C.: The Detection and Attribution Model Intercomparison Project (DAMIP v1.0) contribution to CMIP6, *Geosci. Model. Dev.*, 9, 3685–3697, <https://doi.org/10.5194/gmd-9-3685-2016>, 2016.
- Gillett, N.P., Kirchmeier-Young, M., Ribes, A., Shiogama, H., Hegerl, G.C., Knutti, R., Gastineau, G., John, J.G., Li, L., Nazarenko, L., Rosenbloom, N., Seland, Ø., Wu, T., Yukimoto, S., and Ziehn, T.: Constraining human contributions to
- 645 observed warming since the pre-industrial period, *Nat. Clim. Chang.*, 11, 207–212, [https://doi.org/10.1038/s41558-020-00965-](https://doi.org/10.1038/s41558-020-00965-9)
- [9](https://doi.org/10.1038/s41558-020-00965-9), 2021.
- Good, S. A., Martin, M. J., and Rayner, N. A.: EN4: Quality controlled ocean temperature and salinity profiles and monthly objective analyses with uncertainty estimates, THE EN4 DATA SET, *J. Geophys. Res.-Oceans*, 118, 6704–6716, <https://doi.org/10.1002/2013JC009067>, 2013.
- 650 Gulev, S. K., P. W. Thorne, J. Ahn, F. J. Dentener, C. M. Domingues, S. Gerland, D. Gong, D. S. Kaufman, H. C. Nnamchi, J. Quaas, J.A. Rivera, S. Sathyendranath, S.L. Smith, B. Trewin, K. von Schuckmann, and R. S. Vose: Changing State of the Climate System. In *Climate Change 2021: The Physical Science Basis. Contribution of Working Group I to the Sixth Assessment Report of the Intergovernmental Panel on Climate Change*[Masson-Delmotte, V., P. Zhai, A. Pirani, S.L. Connors, C. Péan, S. Berger, N. Caud, Y. Chen, L. Goldfarb, M.I. Gomis, M. Huang, K. Leitzell, E. Lonnoy, J.B.R. Matthews, T.K.

- 655 Maycock, T. Waterfield, O. Yelekçi, R. Yu, and B. Zhou (eds.)]. Cambridge University Press, Cambridge, United Kingdom and New York, NY, USA, pp. 287–422, <https://doi.org/10.1017/9781009157896.004>, 2021.
- Granier, C., Darras, S., Denier van der Gon, H., Doubalova, J., Elguindi, N., Galle, B., Gauss, M., Guevara, M., Jalkanen, J.-P., Kuenen, J., Liousse, C., Quack, B., Simpson, D., and Sindelarova, K.: The Copernicus Atmosphere Monitoring Service global and regional emissions (April 2019 version), <https://doi.org/10.24380/D0BN-KX16>, n.d, 2019.
- 660 Jalkanen, J.-P., Johansson, L., Kukkonen, J., Brink, A., Kalli, J., and Stipa, T.: Extension of an assessment model of ship traffic exhaust emissions for particulate matter and carbon monoxide, *Atmospheric Chemistry and Physics*, 12, 2641–2659, <https://doi.org/10.5194/acp-12-2641-2012>, 2012.
- Jalkanen, J.-P., Johansson, L., and Kukkonen, J.: A comprehensive inventory of ship traffic exhaust emissions in the European sea areas in 2011, *Atmos. Chem. Phys.*, 16, 71–84, <https://doi.org/10.5194/acp-16-71-2016>, 2016.
- 665 Johansson, L., Jalkanen, J.-P., and Kukkonen, J.: Global assessment of shipping emissions in 2015 on a high spatial and temporal resolution, *Atmospheric Environment*, 167, 403–415, <https://doi.org/10.1016/j.atmosenv.2017.08.042>, 2017.
- Haustein, K., Allen, M. R., Forster, P. M., Otto, F. E. L., Mitchell, D. M., Matthews, H. D., and Frame, D. J.: A real-time Global Warming Index, *Sci Rep*, 7, 15417, <https://doi.org/10.1038/s41598-017-14828-5>, 2017.
- Hersbach H., Bell, B., Berrisford, P. et al.: The ERA5 global reanalysis, *Quat. Jour. R. Met. Soc.*, 146:1999–2049, 670 <https://doi.org/10.1002/qj.3803>, 2020.
- Hodnebrog, Ø., Myhre, G., Kramer, R. J., Shine, K. P., Andrews, T., Faluvegi, G., Kasoar, M., Kirkevåg, A., Lamarque, J.-F., Mülmenstädt, J., Olivieć, D., Samset, B. H., Shindell, D., Smith, C. J., Takemura, T., and Voulgarakis, A.: The effect of rapid adjustments to halocarbons and N₂O on radiative forcing, *npj Clim. Atmos. Sci.*, 3, 43, <https://doi.org/10.1038/s41612-020-00150-x>, 2020a.
- 675 Hodnebrog, Ø., Aamaas, B., Fuglestedt, J. S., Marston, G., Myhre, G., Nielsen, C. J., et al.: Updated global warming potentials and radiative efficiencies of halocarbons and other weak atmospheric absorbers, *Rev. Geophys.*, 58, e2019RG000691, <https://doi.org/10.1029/2019RG000691>, 2020b.
- Hurst, D. F., Oltmans, S. J., Vömel, H., Rosenlof, K. H., Davis, S. M., Ray, E. A., Hall, E. G., and Jordan, A. F.: Stratospheric water vapor trends over Boulder, Colorado: Analysis of the 30 year Boulder record, *J. Geophys. Res.-Atmos.*, 116, 680 <https://doi.org/10.1029/2010JD015065>, 2011.
- Huang, B., Yin, X., Menne, M., Vose, R., and Zhang, H.M.: Improvements to the land surface air temperature reconstruction in NOAA GlobalTemp: An artificial neural network approach, *Artificial Intelligence for the Earth Systems*, 1, 3, <https://journals.ametsoc.org/view/journals/aies/1/4/AIES-D-22-0032.1.xml>, 2020.
- IATA: Global Outlook for Air Transport: Times of Turbulence, IATA, <https://www.iata.org/en/iata-repository/publications/economic-reports/airline-industry-economic-performance---june-2022---report/>, 2022.

- IEA: World oil statistics (Edition 2021), IEA Oil Information Statistics (database), <https://doi.org/10.1787/558987b9-en>, 2022 (accessed on 24 April 2023).
- Ishii, M., Fukuda, Y., Hirahara, S., Yasui, S., Suzuki, T., and Sato, K.: Accuracy of Global Upper Ocean Heat Content Estimation Expected from Present Observational Data Sets, SOLA, 13, 163–167, <https://doi.org/10.2151/sola.2017-030>, 2017.
- 690 Jenkins, S., Smith, C., Allen, M., and Grainger, R.: Tonga eruption increases chance of temporary surface temperature anomaly above 1.5 °C, *Nature Clim. Chang.*, 13, 127–129, <https://doi.org/10.1038/s41558-022-01568-2>, 2023.
- Joshi, M. M. and Jones, G. S.: The climatic effects of the direct injection of water vapour into the stratosphere by large volcanic eruptions, *Atmos. Chem. Phys.*, 9, 6109–6118, <https://doi.org/10.5194/acp-9-6109-2009>, 2009.
- Jungclaus, J. H., Bard, E., Baroni, M., Braconnot, P., Cao, J., Chini, L. P., Egorova, T., Evans, M., González-Rouco, J. F.,
695 Goosse, H., Hurtt, G. C., Joos, F., Kaplan, J. O., Khodri, M., Klein Goldewijk, K., Krivova, N., LeGrande, A. N., Lorenz, S. J., Luterbacher, J., Man, W., Maycock, A. C., Meinshausen, M., Moberg, A., Muscheler, R., Nehrbass-Ahles, C., Otto-Bliesner, B. I., Phipps, S. J., Pongratz, J., Rozanov, E., Schmidt, G. A., Schmidt, H., Schmutz, W., Schurer, A., Shapiro, A. I., Sigl, M., Smerdon, J. E., Solanki, S. K., Timmreck, C., Toohey, M., Usoskin, I. G., Wagner, S., Wu, C.-J., Yeo, K. L., Zanchettin, D., Zhang, Q., and Zorita, E.: The PMIP4 contribution to CMIP6 – Part 3: The last millennium, scientific objective,
700 and experimental design for the PMIP4 past1000 simulations, *Geosci. Model Dev.*, 10, 4005–4033, <https://doi.org/10.5194/gmd-10-4005-2017>, 2017.
- Kadow, C., Hall, D. M., and Ulbrich, U.: Artificial intelligence reconstructs missing climate information, *Nat. Geosci.*, 13, 408–413, <https://doi.org/10.1038/s41561-020-0582-5>, 2020.
- Keeble, J., Hassler, B., Banerjee, A., Checa-Garcia, R., Chiodo, G., Davis, S., Eyring, V., Griffiths, P. T., Morgenstern, O.,
705 Nowack, P., Zeng, G., Zhang, J., Bodeker, G., Burrows, S., Cameron-Smith, P., Cugnet, D., Danek, C., Deushi, M., Horowitz, L. W., Kubin, A., Li, L., Lohmann, G., Michou, M., Mills, M. J., Nabat, P., Olivie, D., Park, S., Seland, Ø., Stoll, J., Wieners, K.-H., and Wu, T.: Evaluating stratospheric ozone and water vapour changes in CMIP6 models from 1850 to 2100, *Atmos. Chem. Phys.*, 21, 5015–5061, <https://doi.org/10.5194/acp-21-5015-2021>, 2021.
- Kovilakam, M., Thomason, L. W., Ernest, N., Rieger, L., Bourassa, A., and Millán, L.: The Global Space-based Stratospheric
710 Aerosol Climatology (version 2.0): 1979–2018, *Earth Syst. Sci. Data*, 12, 2607–2634, <https://doi.org/10.5194/essd-12-2607-2020>, 2020.
- Leach, N. J., Jenkins, S., Nicholls, Z., Smith, C. J., Lynch, J., Cain, M., Walsh, T., Wu, B., Tsutsui, J., and Allen, M. R.: FaIRv2.0.0: a generalized impulse response model for climate uncertainty and future scenario exploration, *Geosci. Model Dev.*, 14, 3007–3036, <https://doi.org/10.5194/gmd-14-3007-2021>, 2021.
- 715 Lee, D. S., Fahey, D. W., Skowron, A., Allen, M. R., Burkhardt, U., Chen, Q., Doherty, S. J., Freeman, S., Forster, P. M., Fuglestedt, J., Gettelman, A., León, R. R. D., Lim, L. L., Lund, M. T., Millar, R. J., Owen, B., Penner, J. E., Pitari, G., Prather,

- M. J., Sausen, R., and Wilcox, L. J.: The contribution of global aviation to anthropogenic climate forcing for 2000 to 2018, *Atmos. Environ.*, 244, 117834, <https://doi.org/10.1016/j.atmosenv.2020.117834>, 2021.
- 720 Lee, J.-Y., J. Marotzke, G. Bala, L. Cao, S. Corti, J.P. Dunne, F. Engelbrecht, E. Fischer, J.C. Fyfe, C. Jones, A. Maycock, J. Mutemi, O. Ndiaye, S. Panickal, and T. Zhou: Future Global Climate: Scenario-Based Projections and Near-Term Information. In *Climate Change 2021: The Physical Science Basis. Contribution of Working Group I to the Sixth Assessment Report of the Intergovernmental Panel on Climate Change*[Masson-Delmotte, V., P. Zhai, A. Pirani, S.L. Connors, C. Péan, S. Berger, N. Caud, Y. Chen, L. Goldfarb, M.I. Gomis, M. Huang, K. Leitzell, E. Lonnoy, J.B.R. Matthews, T.K. Maycock, T. Waterfield, O. Yelekçi, R. Yu, and B. Zhou (eds.)]. Cambridge University Press, Cambridge, United Kingdom and New York, NY, USA, 725 pp. 553–672, <https://doi.org/10.1017/9781009157896.006>, 2021.
- Lee, H., K. Calvin, D. Dasgupta, G. Krinner, A. Mukherji, P. Thorne, C. Trisos, J. Romero, P. Aldunce, K. Barrett, G. Blanco, W.W.L. Cheung, S.L. Connors, F. Denton, A. Diongue-Niang, D. Dodman, M. Garschagen, O. Geden, B. Hayward, C. Jones, F. Jotzo, T. Krug, R. Lasco, J.-Y. Lee, V. Masson-Delmotte, M. Meinshausen, K. Mintenbeck, A. Mokssit, F.E.L. Otto, M. Pathak, A. Pirani, E. Poloczanska, H.-O. Pörtner, A. Revi, D.C. Roberts, J. Roy, A.C. Ruane, J. Skea, P.R. Shukla, R. Slade, 730 A. Slangen, Y. Sokona, A.A. Sörensön, M. Tignor, D. van Vuuren, Y.-M. Wei, H. Winkler, P. Zhai, and Z. Zommers: Synthesis Report of the IPCC Sixth Assessment Report (AR6): Summary for Policymakers. Intergovernmental Panel on Climate Change [accepted], available at <https://www.ipcc.ch/report/ar6/syr/>, 2023.
- Lenssen, N. J. L., Schmidt, G. A., Hansen, J. E., Menne, M. J., Persin, A., Ruedy, R., and Zyss, D.: Improvements in the GISTEMP Uncertainty Model, *J. Geophys. Res.-Atmos.*, 124, 6307–6326, <https://doi.org/10.1029/2018JD029522>, 2019.
- 735 Levitus, S., Antonov, J. I., Boyer, T. P., Baranova, O. K., Garcia, H. E., Locarnini, R. A., Mishonov, A. V., Reagan, J. R., Seidov, D., Yarosh, E. S., and Zweng, M. M.: World ocean heat content and thermosteric sea level change (0–2000 m), 1955–2010, *Geophys. Res. Lett.*, 39, <https://doi.org/10.1029/2012GL051106>, 2012.
- Matthes, K., Funke, B., Andersson, M. E., Barnard, L., Beer, J., Charbonneau, P., Clilverd, M. A., Dudok de Wit, T., Haberreiter, M., Hendry, A., Jackman, C. H., Kretzschmar, M., Kruschke, T., Kunze, M., Langematz, U., Marsh, D. R., 740 Maycock, A. C., Misios, S., Rodger, C. J., Scaife, A. A., Seppälä, A., Shangguan, M., Sinnhuber, M., Tourpali, K., Usoskin, I., van de Kamp, M., Verronen, P. T., and Versick, S.: Solar forcing for CMIP6 (v3.2), *Geosci. Model Dev.*, 10, 2247–2302, <https://doi.org/10.5194/gmd-10-2247-2017>, 2017.
- Meinshausen, M., Nicholls, Z. R. J., Lewis, J., Gidden, M. J., Vogel, E., Freund, M., Beyerle, U., Gessner, C., Nauels, A., Bauer, N., Canadell, J. G., Daniel, J. S., John, A., Krummel, P. B., Luderer, G., Meinshausen, N., Montzka, S. A., Rayner, P. 745 J., Reimann, S., Smith, S. J., van den Berg, M., Velders, G. J. M., Vollmer, M. K., and Wang, R. H. J.: The shared socio-economic pathway (SSP) greenhouse gas concentrations and their extensions to 2500, *Geosci. Model Dev.*, 13, 3571–3605, <https://doi.org/10.5194/gmd-13-3571-2020>, 2020.

- Millán, L., Santee, M. L., Lambert, A., Livesey, N. J., Werner, F., Schwartz, M. J., Pumphrey, H. C., Manney, G. L., Wang, Y., Su, H., Wu, L., Read, W. G., and Froidevaux, L.: The Hunga Tonga-Hunga Ha'apai Hydration of the Stratosphere, *Geophys. Res. Lett.*, 49, e2022GL099381, <https://doi.org/10.1029/2022GL099381>, 2022.
- 750
- Millar, R. J., Nicholls, Z. R., Friedlingstein, P., and Allen, M. R.: A modified impulse-response representation of the global near-surface air temperature and atmospheric concentration response to carbon dioxide emissions, *Atmos. Chem. Phys.*, 17, 7213–7228, <https://doi.org/10.5194/acp-17-7213-2017>, 2017.
- Morice, C. P., Kennedy, J. J., Rayner, N. A., Winn, J. P., Hogan, E., Killick, R. E., Dunn, R. J. H., Osborn, T. J., Jones, P. D., and Simpson, I. R.: An Updated Assessment of Near-Surface Temperature Change From 1850: The HadCRUT5 Data Set, *J. Geophys. Res.-Atmos.*, 126, e2019JD032361, <https://doi.org/10.1029/2019JD032361>, 2021.
- 755
- Myhre, G., Samset, B. H., Schulz, M., Balkanski, Y., Bauer, S., Bernsten, T. K., Bian, H., Bellouin, N., Chin, M., Diehl, T., Easter, R. C., Feichter, J., Ghan, S. J., Hauglustaine, D., Iversen, T., Kinne, S., Kirkevåg, A., Lamarque, J.-F., Lin, G., Liu, X., Lund, M. T., Luo, G., Ma, X., van Noije, T., Penner, J. E., Rasch, P. J., Ruiz, A., Seland, Ø., Skeie, R. B., Stier, P., Takemura, T., Tsigaridis, K., Wang, P., Wang, Z., Xu, L., Yu, H., Yu, F., Yoon, J.-H., Zhang, K., Zhang, H., and Zhou, C.: Radiative forcing of the direct aerosol effect from AeroCom Phase II simulations, *Atmos. Chem. Phys.*, 13, 1853–1877, <https://doi.org/10.5194/acp-13-1853-2013>, 2013a.
- 760
- Myhre, G., D. Shindell, F.-M. Bréon, W. Collins, J. Fuglestedt, J. Huang, D. Koch, J.-F. Lamarque, D. Lee, B. Mendoza, T. Nakajima, A. Robock, G. Stephens, T. Takemura and H. Zhang: Anthropogenic and Natural Radiative Forcing. In: *Climate Change 2013: The Physical Science Basis. Contribution of Working Group I to the Fifth Assessment Report of the Intergovernmental Panel on Climate Change*, edited by Stocker, T.F., D. Qin, G.-K. Plattner, M. Tignor, S.K. Allen, J. Boschung, A. Nauels, Y. Xia, V. Bex and P.M. Midgley (eds.]. Cambridge University Press, Cambridge, United Kingdom and New York, NY, USA, <https://doi.org/10.1017/CBO9781107415324.018>, 2013b.
- 765
- Nicholls Z., Lewis J., Makin M., et al. Regionally aggregated, stitched and de-drifted CMIP-climate data, processed with netCDF-SCM v2.0.0. *Geosci Data J.*, 8, 154–198, <https://doi.org/10.1002/gdj3.113>, 2021
- 770
- Nitzbon, J., Krinner, G., Langer, M.: GCOS EHI 1960-2020 Permafrost Heat Content, World Data Center for Climate (WDCC) at DKRZ, https://doi.org/10.26050/WDCC/GCOS_EHI_1960-2020_PHC, 2022b.
- Otto, F. E. L., Frame, D. J., Otto, A., and Allen, M. R.: Embracing uncertainty in climate change policy, *Nature Clim. Chang.*, 5, 917–920, <https://doi.org/10.1038/nclimate2716>, 2015.
- 775
- Palmer, M. D., Domingues, C. M., Slangen, A. B. A., and Dias, F. B.: An ensemble approach to quantify global mean sea-level rise over the 20th century from tide gauge reconstructions, *Environ. Res. Lett.*, 16, 044043, <https://doi.org/10.1088/1748-9326/abdaec>, 2021.

- Purkey, S.G. and Johnson, G.C., Warming of Global Abyssal and Deep Southern Ocean Waters between the 1990s and 2000s: Contributions to Global Heat and Sea Level Rise Budgets, *J. Climate*, 23, 6336–6351, <https://doi.org/10.1175/2010JCLI3682.1>, 2010.
- 780 Qasmi, S. and Ribes, A.: Reducing uncertainty in local temperature projections, *Sci. Adv.*, 8, eabo6872, <https://doi.org/10.1126/sciadv.abo6872>, 2022.
- Riahi, K., Schaeffer, J. Arango, K. Calvin, C. Guivarch, T. Hasegawa, K. Jiang, E. Kriegler, R. Matthews, G.P. Peters, A. Rao, S. Robertson, A.M. Sebbit, J. Steinberger, M. Tavoni, D.P. van Vuuren, 2022: Mitigation pathways compatible with long-term
- 785 goals. In IPCC, 2022: Climate Change 2022: Mitigation of Climate Change. Contribution of Working Group III to the Sixth Assessment Report of the Intergovernmental Panel on Climate Change [P.R. Shukla, J. Skea, R. Slade, A. Al Khourdajie, R. van Diemen, D. McCollum, M. Pathak, S. Some, P. Vyas, R. Fradera, M. Belkacemi, A. Hasija, G. Lisboa, S. Luz, J. Malley, (eds.)]. Cambridge University Press, Cambridge, UK and New York, NY, USA, <https://doi.org/10.1017/9781009157926.005>, 2022.
- 790 Ribes, A., Planton, S., and Terray, L.: Application of regularised optimal fingerprinting to attribution. Part I: method, properties and idealised analysis, *Clim. Dyn.*, 41, 2817–2836, <https://doi.org/10.1007/s00382-013-1735-7>, 2013.
- Ribes, A., Qasmi, S., and Gillett, N. P.: Making climate projections conditional on historical observations, *Sci. Adv.*, 7, eabc0671, <https://doi.org/10.1126/sciadv.abc0671>, 2021.
- Richardson, M., Cowtan, K., and Millar, R. J.: Global temperature definition affects achievement of long-term climate goals, *Environ. Res. Lett.*, 13, 054004, <https://doi.org/10.1088/1748-9326/aab305>, 2018.
- 795 Rogelj, J., Schaeffer, M., Meinshausen, M., Shindell, D. T., Hare, W., Klimont, Z., Velders, G. J., Amann, M., and Schellnhuber, H. J.: Disentangling the effects of CO₂ and short-lived climate forcer mitigation, *Proc. Natl. Acad. Sci. USA*, 111 (46), 16325–16330, <https://doi.org/10.1073/pnas.1415631111>, 2014a.
- Rogelj, J., D. Shindell, K. Jiang, S. Fifita, P. Forster, V. Ginzburg, C. Handa, H. Khesghi, S. Kobayashi, E. Kriegler, L.
- 800 Mundaca, R. Séférian, and M. V. Vilariño: Mitigation Pathways Compatible with 1.5°C in the Context of Sustainable Development. In: Global Warming of 1.5°C. An IPCC Special Report on the impacts of global warming of 1.5°C above pre-industrial levels and related global greenhouse gas emission pathways, in the context of strengthening the global response to the threat of climate change, sustainable development, and efforts to eradicate poverty [Masson-Delmotte, V., P. Zhai, H.-O. Pörtner, D. Roberts, J. Skea, P.R. Shukla, A. Pirani, W. Moufouma-Okia, C. Péan, R. Pidcock, S. Connors, J. B. R. Matthews,
- 805 Y. Chen, X. Zhou, M. I. Gomis, E. Lonnoy, T. Maycock, M. Tignor, and T. Waterfield (eds.)]. Cambridge University Press, Cambridge, UK and New York, NY, USA, pp. 93-174, <https://doi.org/10.1017/9781009157940.004>, 2018.
- Rogelj, J., Rao, S., McCollum, D. L., Pachauri, S., Klimont, Z., Krey, V., and Riahi, K: Air-pollution emission ranges consistent with the representative concentration pathways, *Nature Clim. Chang.*, 4 (6), 446–450, <https://doi.org/10.1038/nclimate2178>, 2014b.

- 810 Rogelj, J., Lamboll, R.D.: Substantial reductions in non-CO₂ greenhouse gas emissions reductions implied by IPCC estimates of the remaining carbon budget. *Communications Earth Environ* 5, 35. <https://doi.org/10.1038/s43247-023-01168-8>, 2024.
- Rohde, R., Muller, R., Jacobsen, R., Perlmutter, S., Rosenfeld, A., Wurtele, J., Curry, J., Wickham, C., and Mosher, S.: Berkeley Earth temperature averaging process, *Geoinfor. Geostat.: An Overview*, 1, <https://doi.org/10.4172/2327-4581.1000103>, 2013.
- 815 Rohde, R. A. and Hausfather, Z.: The Berkeley Earth Land/Ocean Temperature Record, *Earth Syst. Sci. Data*, 12, 3469–3479, <https://doi.org/10.5194/essd-12-3469-2020>, 2020.
- Sellitto, P., Podglajen, A., Belhadji, R., Boichu, M., Carboni, E., Cuesta, J., Duchamp, C., Kloss, C., Siddans, R., Bègue, N., Blarel, L., Jegou, F., Khaykin, S., Renard, J.B., Legras, B.: The unexpected radiative impact of the Hunga Tonga eruption of 15th January 2022, *Commun. Earth. Environ.*, 3, 288, <https://doi.org/10.1038/s43247-022-00618-z>, 2022.
- 820 von Schuckmann, K., Cheng, L., Palmer, M. D., Hansen, J., Tassone, C., Aich, V., Adusumilli, S., Beltrami, H., Boyer, T., Cuesta-Valero, F. J., Desbruyères, D., Domingues, C., García-García, A., Gentine, P., Gilson, J., Gorfer, M., Haimberger, L., Ishii, M., Johnson, G. C., Killick, R., King, B. A., Kirchengast, G., Kolodziejczyk, N., Lyman, J., Marzeion, B., Mayer, M., Monier, M., Monselesan, D. P., Purkey, S., Roemmich, D., Schweiger, A., Seneviratne, S. I., Shepherd, A., Slater, D. A., Steiner, A. K., Straneo, F., Timmermans, M.-L., and Wjffels, S. E.: Heat stored in the Earth system: where does the energy
- 825 go?, *Earth Syst. Sci. Data*, 12, 2013–2041, <https://doi.org/10.5194/essd-12-2013-2020>, 2020.
- von Schuckmann, K., Minière, A., Gues, F., Cuesta-Valero, F. J., Kirchengast, G., Adusumilli, S., Straneo, F., Ablain, M., Allan, R. P., Barker, P. M., Beltrami, H., Blazquez, A., Boyer, T., Cheng, L., Church, J., Desbruyeres, D., Dolman, H., Domingues, C. M., García-García, A., Giglio, D., Gilson, J. E., Gorfer, M., Haimberger, L., Hakuba, M. Z., Hendricks, S., Hosoda, S., Johnson, G. C., Killick, R., King, B., Kolodziejczyk, N., Korosov, A., Krinner, G., Kuusela, M., Landerer, F. W.,
- 830 Langer, M., Lavergne, T., Lawrence, I., Li, Y., Lyman, J., Marti, F., Marzeion, B., Mayer, M., MacDougall, A. H., McDougall, T., Monselesan, D. P., Nitzbon, J., Otosaka, I., Peng, J., Purkey, S., Roemmich, D., Sato, K., Sato, K., Savita, A., Schweiger, A., Shepherd, A., Seneviratne, S. I., Simons, L., Slater, D. A., Slater, T., Steiner, A. K., Suga, T., Szekely, T., Thiery, W., Timmermans, M.-L., Vanderkelen, I., Wjffels, S. E., Wu, T., and Zemp, M.: Heat stored in the Earth system 1960–2020: where does the energy go?, *Earth System Science Data*, 15, 1675–1709, <https://doi.org/10.5194/essd-15-1675-2023>, 2023.
- 835 Sigl, M., Toohey, M., McConnell, J. R., Cole-Dai, J., and Severi, M.: Volcanic stratospheric sulfur injections and aerosol optical depth during the Holocene (past 11\,500 years) from a bipolar ice-core array, *Earth Syst. Sci. Data*, 14, 3167–3196, <https://doi.org/10.5194/essd-14-3167-2022>, 2022.
- Skeie, R. B., Myhre, G., Hodnebrog, Ø., Cameron-Smith, P. J., Deushi, M., Hegglin, M. I., Horowitz, L. W., Kramer, R. J., Michou, M., Mills, M. J., Olivíe, D. J. L., Connor, F. M. O., Paynter, D., Samset, B. H., Sellar, A., Shindell, D., Takemura, T.,
- 840 Tilmes, S., and Wu, T.: Historical total ozone radiative forcing derived from CMIP6 simulations, *npj Clim. Atmos. Sci.*, 3, 32, <https://doi.org/10.1038/s41612-020-00131-0>, 2020.

- Smith, C. J., Kramer, R. J., Myhre, G., Forster, P. M., Soden, B. J., Andrews, T., Boucher, O., Faluvegi, G., Fläschner, D., Hodnebrog, Ø., Kasoar, M., Kharin, V., Kirkevåg, A., Lamarque, J.-F., Mülmenstädt, J., Olivié, D., Richardson, T., Samset, B. H., Shindell, D., Stier, P., Takemura, T., Voulgarakis, A., and Watson-Parris, D.: Understanding Rapid Adjustments to
845 Diverse Forcing Agents, *Geophys. Res. Lett.*, 45, 12,023–12,031, <https://doi.org/10.1029/2018GL079826>, 2018a.
- Smith, C. J., Forster, P. M., Allen, M., Leach, N., Millar, R. J., Passerello, G. A., and Regayre, L. A.: FAIR v1.3: A simple emissions-based impulse response and carbon cycle model, *Geoscientific Model Development*, 11, 2273–2297, <https://doi.org/10.5194/gmd-11-2273-2018>, 2018b.
- Smith, C. J., Harris, G. R., Palmer, M. D., Bellouin, N., Collins, W., Myhre, G., Schulz, M., Golaz, J.-C., Ringer, M.,
850 Storelvmo, T., and Forster, P. M.: Energy Budget Constraints on the Time History of Aerosol Forcing and Climate Sensitivity, *Journal of Geophysical Research: Atmospheres*, 126, e2020JD033622, <https://doi.org/10.1029/2020JD033622>, 2021a.
- Smith, C., Nicholls, Z. R. J., Armour, K., Collins, W., Forster, P., Meinshausen, M., Palmer, M. D., and Watanabe, M.: The Earth's Energy Budget, Climate Feedbacks, and Climate Sensitivity Supplementary Material, in: *Climate Change 2021: The Physical Science Basis. Contribution of Working Group I to the Sixth Assessment Report of the Intergovernmental Panel on*
855 *Climate Change*, edited by: Masson-Delmotte, V., Zhai, P., Pirani, A., Connors, S. L., Péan, C., Berger, S., Caud, N., Chen, Y., Goldfarb, L., Gomis, M. I., Huang, M., Leitzell, K., Lonnoy, E., Matthews, J. B. R., Maycock, T. K., Waterfield, T., Yelekçi, O., Yu, R., and Zhou, B., 2021b.
- Stevenson, D. S., Young, P. J., Naik, V., Lamarque, J.-F., Shindell, D. T., Voulgarakis, A., Skeie, R. B., Dalsoren, S. B., Myhre, G., Berntsen, T. K., Folberth, G. A., Rumbold, S. T., Collins, W. J., MacKenzie, I. A., Doherty, R. M., Zeng, G., van
860 Noije, T. P. C., Strunk, A., Bergmann, D., Cameron-Smith, P., Plummer, D. A., Strode, S. A., Horowitz, L., Lee, Y. H., Szopa, S., Sudo, K., Nagashima, T., Josse, B., Cionni, I., Righi, M., Eyring, V., Conley, A., Bowman, K. W., Wild, O., and Archibald, A.: Tropospheric ozone changes, radiative forcing and attribution to emissions in the Atmospheric Chemistry and Climate Model Intercomparison Project (ACCMIP), *Atmos. Chem. Phys.*, 13, 3063–3085, <https://doi.org/10.5194/acp-13-3063-2013>, 2013.
- 865 Steiner, A. K., Ladstädter, F., Randel, W. J., Maycock, A. C., Fu, Q., Claud, C., Gleisner, H., Haimberger, L., Ho, S.-P., Keckhut, P., Leblanc, T., Mears, C., Polvani, L. M., Santer, B. D., Schmidt, T., Sofieva, V., Wing, R., and Zou, C.-Z.: Observed Temperature Changes in the Troposphere and Stratosphere from 1979 to 2018, *J. Climate*, 33, 8165–8194, <https://doi.org/10.1175/JCLI-D-19-0998.1>, 2020.
- Sun, W., Li, Q., Huang, B., Cheng, J., Song, Z., Li, H., Dong, W., Zhai, P., and Jones, P.: The Assessment of Global Surface
870 Temperature Change from 1850s: The C-LSAT2.0 Ensemble and the CMST-Interim Datasets, *Advances in Atmospheric Sciences*, 38, 875–888, <https://doi.org/10.1007/s00376-021-1012-3>, 2021.
- Szopa, S., V. Naik, B. Adhikary, P. Artaxo, T. Berntsen, W.D. Collins, S. Fuzzi, L. Gallardo, A. Kiendler-Scharr, Z. Klimont, H. Liao, N. Unger, and P. Zanis: Short-Lived Climate Forcers. In *Climate Change 2021: The Physical Science Basis*.

- Contribution of Working Group I to the Sixth Assessment Report of the Intergovernmental Panel on Climate Change [Masson-Delmotte, V., P. Zhai, A. Pirani, S.L. Connors, C. Péan, S. Berger, N. Caud, Y. Chen, L. Goldfarb, M.I. Gomis, M. Huang, K. Leitzell, E. Lonnoy, J.B.R. Matthews, T.K. Maycock, T. Waterfield, O. Yelekçi, R. Yu, and B. Zhou (eds.)]. Cambridge University Press, Cambridge, United Kingdom and New York, NY, USA, pp. 817–922, <https://doi.org/10.1017/9781009157896.008>, 2021.
- 875 Taha, G., Loughman, R., Zhu, T., Thomason, L., Kar, J., Rieger, L., and Bourassa, A.: OMPS LP Version 2.0 multi-wavelength aerosol extinction coefficient retrieval algorithm, *Atmos. Meas. Tech.*, 14, 1015–1036, <https://doi.org/10.5194/amt-14-1015-2021>, 2021.
- 880 Taylor, K. E., Crucifix, M., Braconnot, P., Hewitt, C. D., Doutriaux, C., Broccoli, A. J., Mitchell, J. F. B., and Webb, M. J.: Estimating Shortwave Radiative Forcing and Response in Climate Models, *J. Climate*, 20, 2530–2543, <https://doi.org/10.1175/JCLI4143.1>, 2007.
- 885 Thomason, L. W., Ernest, N., Millán, L., Rieger, L., Bourassa, A., Vernier, J.-P., Manney, G., Luo, B., Arfeuille, F., and Peter, T.: A global space-based stratospheric aerosol climatology: 1979–2016, *Earth Syst. Sci. Dat.*, 10, 469–492, <https://doi.org/10.5194/essd-10-469-2018>, 2018.
- Thornhill, G. D., Collins, W. J., Kramer, R. J., Olivié, D., Skeie, R. B., O'Connor, F. M., Abraham, N. L., Checa-Garcia, R., Bauer, S. E., Deushi, M., Emmons, L. K., Forster, P. M., Horowitz, L. W., Johnson, B., Keeble, J., Lamarque, J.-F., Michou, 890 M., Mills, M. J., Mulcahy, J. P., Myhre, G., Nabat, P., Naik, V., Oshima, N., Schulz, M., Smith, C. J., Takemura, T., Tilmes, S., Wu, T., Zeng, G., and Zhang, J.: Effective radiative forcing from emissions of reactive gases and aerosols – a multi-model comparison, *Atmos. Chem. Phys.*, 21, 853–874, <https://doi.org/10.5194/acp-21-853-2021>, 2021a.
- Thornhill, G., Collins, W., Olivié, D., Skeie, R. B., Archibald, A., Bauer, S., Checa-Garcia, R., Fiedler, S., Folberth, G., Gjermundsen, A., Horowitz, L., Lamarque, J.-F., Michou, M., Mulcahy, J., Nabat, P., Naik, V., O'Connor, F. M., Paulot, F., 895 Schulz, M., Scott, C. E., Séférian, R., Smith, C., Takemura, T., Tilmes, S., Tsigaridis, K., and Weber, J.: Climate-driven chemistry and aerosol feedbacks in CMIP6 Earth system models, *Atmos. Chem. Phys.*, 21, 1105–1126, <https://doi.org/10.5194/acp-21-1105-2021>, 2021b.
- Toohey, M. and Sigl, M.: Volcanic stratospheric sulfur injections and aerosol optical depth from 500\,BCE to 1900\,CE, *Earth Syst. Sci. Data*, 9, 809–831, <https://doi.org/10.5194/essd-9-809-2017>, 2017.
- 900 Trewin, B., Cazenave, A., Howell, S., Huss, M., Isensee, K., Palmer, M. D., Tarasova, O., and Vermeulen, A.: *Headline Indicators for Global Climate Monitoring*, *Bulletin of the American Meteorological Society*, 102, E20–E37, <https://doi.org/10.1175/BAMS-D-19-0196.1>, 2021.
- Vanderkelen, I., van Lipzig, N. P. M., Lawrence, D. M., Droppers, B., Golub, M., Gosling, S. N., Janssen, A. B. G., Marcé, R., Schmied, H. M., Perroud, M., Pierson, D., Pokhrel, Y., Satoh, Y., Schewe, J., Seneviratne, S. I., Stepanenko, V. M., Tan,

- 905 Z., Woolway, R. I., and Thiery, W.: Global Heat Uptake by Inland Waters, *Geophysical Research Letters*, 47, e2020GL087867, <https://doi.org/10.1029/2020GL087867>, 2020.
- Vose, R. S., Huang, B., Yin, X., Arndt, D., Easterling, D. R., Lawrimore, J. H., Menne, M. J., Sanchez-Lugo, A., and Zhang, H. M.: Implementing Full Spatial Coverage in NOAA’s Global Temperature Analysis, *Geophys. Res. Lett.*, 48, e2020GL090873, <https://doi.org/10.1029/2020GL090873>, 2021.
- 910 Watson-Parris, D., Christensen, M. W., Laurensen, A., Clewley, D., Gryspeerdt, E., and Stier, P.: Shipping regulations lead to large reduction in cloud perturbations, *Proc. Natl. Acad. Sci. U.S.A.*, 119, e2206885119, <https://doi.org/10.1073/pnas.2206885119>, 2022.
- Yuan, T., Song, H., Wood, R., Wang, C., Oreopoulos, L., Platnick, S. E., Von Hippel, S., Meyer, K., Light, S., and Wilcox, E.: Global reduction in ship-tracks from sulfur regulations for shipping fuel, *Sci. Adv.*, 8, eabn7988, <https://doi.org/10.1126/sciadv.abn7988>, 2022.
- 915 Zelinka, M. D., Andrews, T., Forster, P. M., and Taylor, K. E.: Quantifying components of aerosol-cloud-radiation interactions in climate models, *J. Geophys. Res.-Atmos.*, 119, 7599–7615, <https://doi.org/10.1002/2014JD021710>, 2014.
- Zelinka, M. D., Smith, C. J., Qin, Y., and Taylor, K. E.: Aerosol Effective Radiative Forcings in CMIP Models, *EGUsphere*, <https://acp.copernicus.org/articles/23/8879/2023>, 2023.

920